

# Benefits of the Margules Uncertainty Method

*Paul M. Mathias*  
PaulMMathias Consulting, LLC<sup>©</sup>  
[PaulMMathias@Gmail.com](mailto:PaulMMathias@Gmail.com)

ABSTRACT : It is universally recognized by experts that the computer-based design of chemical processes depends strongly on the correlated thermodynamic and transport properties, and the effect of property uncertainties should be propagated into the process design and analysis. Many approaches have been proposed, but uncertainty analysis is not a routine component of today's industrial practice, mainly because education and awareness is lacking, and the proposed methods are difficult to apply. The most significant source of property uncertainties on process design comes from the correlations of mixture phase equilibrium. The author proposed the Margules Uncertainty Method (MUM) in 2014 as a practical way to evaluate the effect of mixture phase-equilibrium uncertainties, and this approach has been applied to six case studies in five peer-reviewed journal publications. An essential feature of the uncertainty-evaluation procedure is detailed data analysis. The key results of these case studies are summarized in this paper to spotlight the many ways in which the MUM – and uncertainty analysis in general – can provide broad value to chemical process technology.

KEYWORDS: vapor-liquid-liquid equilibrium, phase-equilibrium uncertainty, distillation, absorption, risk quantification

## Introduction

Quantifying the uncertainty in physical properties is recognized as being of foremost importance by scientists and technologists in academia and the chemical industry. In a forward to the *Guidelines for Evaluating and Expressing the Uncertainty of NIST Measurement Results*,<sup>1</sup> the then-director of NIST, Dr. John W. Lyons, wrote, “It is generally agreed that the usefulness of measurement results, and thus much of the information that we provide as an institution is, to a large extent, determined by the quality of the statements of uncertainty that accompany them.” Five prominent journals in the field of thermodynamics (*Journal of Chemical and Engineering Data*, *Journal of Chemical Thermodynamics*, *Fluid Phase Equilibria*, *Thermochimica Acta*, and *the International Journal of Thermophysics*) have mandated reporting of combined uncertainties together with the experimental data tables.<sup>2,3,4,5,6,7</sup> Kim et al.<sup>8</sup> highlighted the availability of online resources as an enabler to incorporate uncertainty analysis into chemical-engineering education.

The design of chemical processes today invariably uses computer simulations, and several technologists have identified the need to understand and evaluate the impact of uncertainties in property models on process design and plant operability. Streich and Kistenmacher<sup>9</sup> pointed out that physical properties are of “unequal importance,” and tend to be most important under low-temperature conditions. Mah<sup>10</sup> has shown that in some cases rough approximations of physical properties are quite adequate. By “unequal importance,” Streich and Kistenmacher meant that in some cases there is extreme sensitivity of design to physical properties, and in other cases, the design is insensitive to property uncertainties; the latter is Mah’s observation. Many studies have illustrated the effects of the uncertainty in physical-property models on process design,<sup>11,12,13</sup> however these publications do not provide a practical way to routinely quantify the propagation of property uncertainty into design variability. Macchietto, Maduabeuke and Szcpanski<sup>14</sup> developed a method to connect exact derivatives of calculated properties to flowsheet simulations (e.g., derivative of ethylene purity in an ethylene/ethane superfractionator to the ethane-ethylene binary interaction parameter), and presented examples to demonstrate “that very valuable information can be obtained as to which properties matter in a process and where;” however, this methodology has not been implemented in commercial process-simulation software. Whiting and co-workers made extensive efforts to emphasize the importance of understanding uncertainties in physical properties, and to quantify their effect on process design and plant operation.<sup>15,16,17,18,19,20</sup> For example, they demonstrated strategies for quantification of process uncertainties caused by property uncertainties via Monte Carlo simulations. Miller et al.<sup>21</sup> presented a case study demonstrating that advanced multiscale modeling, including uncertainty quantification, have the capability to dramatically reduce the time and cost to develop new carbon-capture technologies

While the importance of property uncertainty analysis is clearly recognized in the thermodynamics literature, it is hardly used in chemical-engineering practice; as Kim et al.<sup>8</sup> observed, “Its practical implementation in a variety of scientific and engineering fields has typically seen less emphasis than it deserves.” There are several barriers to adopting quantitative uncertainty analysis in chemical-engineering industrial practice. Kim et al.<sup>8</sup> identified education as a key barrier, and proposed the use of online properties with clearly identified uncertainties as the means to integrate uncertainty analysis into undergraduate and graduate courses. Another barrier is that the methods proposed by researchers such as Macchietto, Maduabeuke and Szcpaniski,<sup>14</sup> Whiting and co-workers,<sup>15,16,17,18,19,20</sup> and Miller et al.<sup>21</sup> are not yet easily available in commercial process simulators. A key barrier in our experience is that simple, intuitive methods to perturb properties in a manner consistent with uncertainties are not available, and the purpose of this paper is to describe such a method and to demonstrate its value through a variety of case studies.

Fair<sup>22</sup> presented a table that showed typical errors in physical properties, and offered a rough guide to the effect of inaccurate physical-property values on uncertainty in operating and capital costs. In general, the operating and capital cost variability is approximately proportionate and equivalent to property uncertainty; for example, an uncertainty of 15% in heat of vaporization leads to 15% uncertainties in equipment size and cost, and a 20% uncertainty in density causes 16% uncertainty in equipment size and operating cost. Phase equilibrium is distinctly different because, as shown in Figure 1 (taken from Table 8 in Fair’s paper<sup>22</sup>), the cost of phase-equilibrium inaccuracy increases exponentially as the relative volatility approaches unity. This conclusion is broadly understood and accepted in university courses and the practice of process technology; however, as is shown in this paper, the uncertainty in size and cost due to phase-equilibrium inaccuracy is also dependent on product purity, with diminished sensitivity to property inaccuracy when product purity is relaxed. It is thus necessary to perform the uncertainty analysis for each case, and hence a practical and easily applicable method is needed.

The Margules Uncertainty Method (MUM) is first described. The first step in application of the method is detailed analysis and quantification of the phase-equilibrium uncertainty. This is an essential first step – and its importance cannot be overemphasized, especially since the widespread availability of commercial software has diminished the familiarity of engineers with the underlying data. The six case studies are next summarized as each one provides different insights, and together they present a broad picture of the value of the MUM, and uncertainty analysis in general.

## **Margules-Based Activity-Coefficient Perturbation Scheme**

The phase-equilibrium model used may be based upon an equation of state (in which the same model described all phases in equilibrium) or the hybrid approach (in which the vapor phase is modeled using an equation of state and the liquid phase is described by an activity-coefficient model); for example see Poling, Prausnitz and O’Connell.<sup>23</sup> The hybrid approach is used here, and it is assumed that the predominant phase-equilibrium uncertainty results from the activity-coefficient model.

The MUM perturbation scheme for the activity-coefficient model, first published by Mathias,<sup>24</sup> uses the framework that an extra term is added to each component activity coefficient calculated by the model, and the form of the perturbed activity coefficients is guided by the Margules equation.

$$\ln(\gamma_i) = \ln(\gamma_i^m) + \ln(\gamma_i^p) \quad (1)$$

where  $\gamma_i$  is the activity coefficient of component  $i$  after perturbation,  $\gamma_i^m$  is the activity coefficient calculated by the chosen model (the “best” model in the region of interest should be used), and  $\gamma_i^p$  represents the perturbation obtained through the estimated model uncertainty. It should be emphasized that  $\gamma_i^m$  is calculated from the “best” activity-coefficient model, and is not in any way restricted by the form chosen for  $\gamma_i^p$ .  $\gamma_i^p$  is guided by the form of the Margules equation, and is given by,

$$\ln(\gamma_i^p) = \delta_i (1-x_i)^2 \left[ \frac{|\ln(\gamma_i^m)|}{(1-x_i)^2 + |\ln(\gamma_i^m)|} \right] \quad (2)$$

Equation 2 is phenomenological, but has desired characteristics. The value of  $\ln(\gamma_i^p)$  is small when  $\gamma_i^m$  is close to unity (i.e., low departures from ideal behavior), and also is low when the mole fraction of component  $i$  is close to unity. For components at concentrations close to infinite dilution and with activity coefficients significantly different from unity, the fractional change in  $\gamma_i$  resulting from the perturbation asymptotically approaches  $\{exp(\delta_i) - 1\}$ . In order to apply the perturbation method, the value of  $\delta_i$  for each component, or for groups of components, must be related to the estimated uncertainty in its activity coefficient, determined by thorough phase-equilibrium data analysis. This thorough data analysis is an essential element of the perturbation scheme.

Figure 2 shows the percentage change in the infinite-dilution activity coefficient as a function of the infinite-dilution activity coefficient  $\gamma^{m\infty}$  and the perturbation parameter  $\delta$ , and gives an indication about the range of values of component  $\delta$ 's to be chosen for a particular case. As will be seen, for example, in Dehexanizer Column, the largest values of the infinite-dilution activity coefficients are in the range 1.5 to 2, and estimated uncertainties in the activity coefficients is about 5%. Thus an appropriate range of  $\delta$  values to be studied for this case – and applied to all components – is between +0.2 and -0.2.

## Implementation of Margules Uncertainty Method (MUM)

The perturbation scheme has been implemented in Aspen Plus as a user activity-coefficient model that adds the perturbation capability to the NRTL-RK property option; however, it should be noted that the framework could be applied to any activity-coefficient model in any commercial process-simulation software. The NRTL-RK property option uses the NRTL activity-coefficient model<sup>25</sup> and the Redlich-Kwong equation of state<sup>26</sup> for the vapor phase. The pure-component properties come from the DIPPR 801 database,<sup>27</sup> and the chemicals in all six case studies are well studied, and hence their vapor pressures are expected to be accurate, better than 1 %. The vapor-phase fugacity coefficient appears in the vapor and liquid fugacities (in the liquid it converts the pure-component vapor pressure into the pure-liquid fugacity<sup>23</sup>), and the two fugacity coefficients tend to cancel when all boiling points are similar. Further, all applications here are at about ambient pressure, hence the vapor-phase fugacity coefficients are close to unity. Therefore, the phase-equilibrium uncertainty is principally determined by the uncertainties in the component activity coefficients.

The NRTL model has two temperature-dependent binary parameters ( $\alpha_{ij}^N$  and  $\tau_{ij}$ ).  $\alpha_{ij}^N$  is a symmetric binary parameter and  $\tau_{ij}$  is an asymmetric binary parameter,

$$\tau_{ij} = a_{ij} + b_{ij}/T + e_{ij} \ln(T) + f_{ij}T \quad (3)$$

$$\alpha_{ij}^N = c_{ij} + d_{ij}(T - 273.15) \quad (4)$$

where, T is the temperature in Kelvin.

The K-value of component  $i$  in a mixture ( $K_i$ ) at vapor-liquid equilibrium (VLE) is defined to be the ratio of its vapor and liquid mole fractions at equilibrium, and the relative volatility between components  $i$  and  $j$  ( $\alpha_{ij}$ ) is the ratio of the two K-values.

$$K_i \equiv \frac{y_i}{x_i} \quad (5)$$

$$\alpha_{ij} \equiv \frac{K_i}{K_j} \quad (6)$$

Note that the superscript “*N*” has been added to the NRTL parameter  $\alpha_{ij}^N$  (Eq. 4) in order to distinguish it from the relative volatility,  $\alpha_{ij}$ .

The Data Regression System (DRS) in Aspen Plus has been used to determine optimum values of the NRTL parameters (eqs 3 and 4), as described in the primary publications. Phase-equilibrium data were obtained from the NIST-TDE<sup>28</sup> database, the Dortmund databank,<sup>29</sup> and other sources, and also key VLE data have been measured in one case study. In one case study (Dehexanizer Column), some of the NRTL parameters were estimated by the UNIFAC method.<sup>30</sup> Brief overviews on the source of the NRTL binary parameters are summarized here in each of the six cases, and these are described in detail in the primary publications.

## Analysis of Phase-Equilibrium Data

The importance of thorough analysis of the phase-equilibrium data as the first step must be strongly reiterated. It is also important that the data be analyzed as distribution coefficients (e.g., K-values) in addition to the customary temperature-pressure-composition diagrams. The primary publications of the case studies have already presented the detailed data analysis, hence, in the interests of brevity, only the highlights are given here.

Mathias<sup>31</sup> showed that the practice of representing VLE data through the use of state conditions (temperature and pressure) and phase compositions does not reveal and quantify the accuracy of the data for important purposes, such as separation by distillation. VLE data should be evaluated through the use of distribution coefficients, like K-values and relative volatilities. Figure 3 compares calculations from the correlated NRTL-RK property option with the data of Kojima et al.<sup>32</sup> for the acetone + chloroform binary mixture at 101.3 kPa using a *Txy* diagram. The results illustrate that the agreement between model and data is good, and that both the model and data clearly depict the maximum-boiling azeotrope, but charts like Figure 3 are unable to provide quantitative uncertainty estimates, and are particularly weak in this respect at the two pure ends. Figure 4 compares calculated relative volatilities for the same acetone + chloroform binary at 101.3 kPa with data from Kudryavtseva and Kusarev,<sup>33</sup> Kogan and Deizenrot,<sup>34</sup> Kojima et al.,<sup>32</sup> and Segura et al.<sup>35</sup> The data from all four sources agree well (except for two outliers from Kogan and Diezenrot,<sup>34</sup> which are readily identified), and the chart clearly demonstrates that the combined model uncertainty (about three standard deviations) is 5%. Figure 3 is

effective in showing the existence of the azeotrope, but Figure 4 is far superior since it enables quantification of model and data uncertainties at a glance, and is an effective way to communicate such information to a human. Figure 5 shows a comparable way to visualize information analogous to Figure 4 for ternary and higher mixtures; it presents percentage differences between acetone K-values from model and data plotted against the mole fraction of acetone. We expect the most interesting and relevant comparisons at low concentrations. Indeed, review of Figure 5 shows that the model K-values agree with the data of Kojima et al.<sup>32</sup> to within  $\pm 5\%$ , but the deviations from the data of Reinders and de Minjer<sup>36</sup> are much larger, suggesting greater uncertainty of the latter data set. Figure 4 and Figure 5 are clearly better than Figure 3 since they enable visual inspection of the model and data uncertainty, and estimation of the correlation uncertainty. Here, if the Reinders and de Minjer data<sup>36</sup> are ignored, it is clear that the uncertainties are better than  $\pm 5\%$ , and 5 % may be considered to be three standard deviations (i.e., 99.7% of all measured data). It is for this reason that the *Journal of chemical & Engineering Data* has stipulated<sup>31</sup> that analysis of VLE data must include distribution coefficients, such as K-values and relative volatilities. The phase-equilibrium data in all six case studies presented in this paper have been analyzed using distribution coefficients.

## Case Studies

The six case studies are summarized next. In the interests of brevity, the discussion is limited to problem statement and a discussion of the key results. Readers who wish to find out the details are urged to study the primary publications.

### Case Study 1: C<sub>3</sub> Splitter.

Propane-propylene splitters separate a close-boiling mixture (relative volatility could be 1.1, or even closer to unity), and are therefore highly sensitive to the phase-equilibrium correlation. Streich and Kistenmacher<sup>9</sup> wrote, “If the process engineer must know the number of theoretical trays in the C<sub>2</sub> or C<sub>3</sub> splitters within 5%, he will have to predict the K-values for ethane within 0.6% and the K-values for propane within 0.3%. We will define the accuracy level for a tray number within 5% as the ‘desirable accuracy.’” Mathias<sup>24</sup> applied the MUM to a representative C<sub>3</sub> splitter. First, it was determined through careful data analysis that the uncertainty in the correlation relative volatility is  $\pm 1\%$ , and this represents 3 standard deviations. The design case chosen was a column with 116 theoretical stages, including a condenser and a reboiler, operating at 125 psig (963 kPa). The feed rate is 1,000 kmol/h and is an equimolar mixture of propane and propylene at its bubble point at 963 kPa, and the feed stage is # 75, numbered from the top. The base column specifications are 0.99 mol fraction propylene as distillate and

0.97 mol fraction propane as bottoms. The calculated condenser and reboiler duties for the base case are -125.7 GJ/h and 123.4 GJ/h, respectively.

The relative volatilities at the top (propylene rich) and bottom (propane rich) of the column are 1.1 and 1.27, respectively, and hence (Figure 1) we expect greater sensitivity to VLE uncertainty at the top (propylene-rich end) than at the bottom (propane-rich end). Figure 6 presents the effect of perturbing the infinite-dilution propylene activity coefficient (or equivalently, the relative volatility at the propane-rich end) on the reboiler duty at four values of the propane purity (concentration of propylene in the propane product). In all cases, the distillate concentration was fixed at 99 mol% propylene. At the base purity of 0.03 mol fraction propylene in propane, a 1 % reduction in the relative volatility causes 1 % increase in the reboiler duty, and if the purity is modified to 0.005 mol fraction propylene in propane, the increased uncertainty in reboiler duty is 2.7 %. Figure 7 presents analogous results of perturbing the relative volatility at the propylene-rich end, and the uncertainty effects for this case are significantly higher. Here, a 1 % reduction in the relative volatility for the base case of 0.01 mol fraction propane in propylene causes 13 % increase in reboiler duty, and the increase rises to 28 % if the propylene purity specification is fixed at a mole fraction of 0.998. These results are, of course, qualitatively expected;<sup>9, 22</sup> however, the value of the MUM framework is that the design engineer can quickly and easily make quantitative estimates of the effect of phase equilibrium on process design for any specific design case. Another important conclusion from Figure 7 is that if the propylene purity is reduced to a mole fraction of 0.95, which corresponds to chemical-grade, rather than polymer-grade propylene, the sensitivity of reboiler duty to uncertainties in relative volatility is reduced considerably, to about 4 %. While one would expect lower sensitivity of design as the product purity is lowered, the MUM framework enables quantitative estimates for the specific case of interest.

## Case Study 2: Dehexanizer Column.

Dehexanizer columns remove C<sub>5</sub> and C<sub>6</sub> paraffins from a heavier slate of compounds that are mostly aromatic. The number of components in the simulation is usually quite large, and Mathias<sup>24</sup> presented results for a case with 61 components, and with normal boiling points ranging from 231 K (propane) to 479 K (n-pentylbenzene). The analysis of phase equilibrium concluded that the uncertainty in pure-component vapor pressures for this system is about 1%, while the uncertainty in the activity coefficients (using fitting of VLE data as well as estimations using the UNIFAC group-contribution method<sup>30</sup>) is about 5%.

The column has 30 theoretical stages, including a reboiler and a total condenser, and the feed tray is # 23, numbered from the top. The condenser pressure is 160 kPa, the reboiler pressure is 227 kPa, the pressure drop in the condenser is 2.9 kPa, and the pressure drop is equal over the other trays. The column spec is 0.02 mole fraction heavies ( $T_b > 352$ ) in the distillate, and 0.02 mole fraction lights ( $T_b < 352$  K) in the bottoms.

Figure 8 indicates how components split to the distillate as a function of normal boiling point. The boiling points of interest are in the range of 323 to 359 K, since lighter components ( $T_b < 323$  K) split predominantly to the distillate, and heavier components ( $T_b > 359$  K) report almost totally to the bottoms. As expected, the split to the distillate decreases as the normal boiling point increases. The curve shown follows the paraffinic compounds (except benzene), and it is clear that the split of benzene to the distillate is greater than would be predicted based upon vapor pressure alone. Figure 9 presents the activity coefficients of selected compounds as a function of the stage number of the Dehexanizer Column. Above the feed stage the mixture is dominated by the paraffinic compounds, and hence the activity coefficients of the paraffins are close to unity, while the activity coefficient of benzene is greater than unity. This result explains why the split of benzene to the distillate is higher than expected based upon vapor pressure alone. Below the feed tray the mixture is mostly aromatic, and therefore benzene has an activity coefficient close to unity while the activity coefficients of the paraffinic compounds are greater than unity.

The uncertainty in the activity coefficients is estimated to be  $\pm 5\%$  (corresponding to about two standard deviations), and the largest activity coefficients are between 1.5 and 2, hence an appropriate range for the values of  $\delta_i$  is between -0.2 and 0.2 (Figure 2). The question is how best to apply the MUM perturbations since there are many components in the system. It was concluded that one value of the perturbation could be applied to all the light components, and another value of the perturbation would be applied to all the heavy components. The base case is the one where no perturbation has been applied. Other cases are identified by up and down arrows. An up arrow ( $\uparrow$ ) means that the component  $\delta$  values (and consequently K-values) have been increased, while a down arrow ( $\downarrow$ ) means that the component  $\delta$  values have been decreased. The first arrow refers to the heavies and the second arrow refers to the lights. For example,  $\uparrow\downarrow$  means that the  $\delta$  values of the heavies have been increased and the  $\delta$  values of the lights have been decreased. The results of the results of the four possible perturbations are presented in Table 1.

**Table 1. Effect of Activity-Coefficient Perturbation on Dehexanizer Column design. Figure reprinted with permission from ref 24. Copyright 2014 ACS.**

Case	$\delta$ -Heavies	$\delta$ -Lights	Reflux Ratio	Boilup Ratio	Reboiler Duty (Gcal/h)	Condenser Duty (Gcal/h)	% Change in Reboiler Duty	% Change in Condenser Duty
Base	0	0	3.139	0.847	5.009	-3.920	0.0	0.0
↑↑	0.20	0.20	3.125	0.837	4.968	-3.905	-0.8	-0.4
↓↓	-0.20	-0.20	3.171	0.859	5.068	-3.952	1.2	0.8
↓↑	-0.20	0.20	2.855	0.805	4.760	-3.649	-5.0	-6.9
↑↓	0.20	-0.20	3.505	0.901	5.337	-4.269	6.5	8.9

Examination of the results in Table 1 enables the following insights:

1. Changing the activity coefficients of the heavies and lights in the same direction (Cases ↑↑ and ↓↓) has only a small effect on the column design. This is to be expected since ↑↑ improves the stripping section and hurts the rectifying section, while ↓↓ has the opposite effect, but it is reassuring that the model gives this expected result.
2. Lowering the activity coefficients of the heavies and raising the activity coefficients of the lights (Case ↓↑) reduces the reboiler and condenser duties, i.e., an optimistic design. Again, this is an expected result (both the stripping and rectifying sections are improved), but obtaining expected results increases confidence in the approach used here.
3. Finally, raising the activity coefficients of the heavies and lowering the activity coefficients of the lights results in a conservative design. Perturbing the activity coefficients by about 5%, results in increases in the reboiler and condenser duties by 7% and 9%, respectively. Hence the approach used here provides a quantitative relationship between the activity coefficient uncertainty and the column design variability.

The Dehexanizer Column example illustrates that even for a system containing many components, the MUM framework clarifies the key uncertainties and facilitates a quantitative relationship between phase-equilibrium uncertainties and the variability in the design. The uncertainties in the Dehexanizer Column are about an order of magnitude higher than for the propane-propylene splitter, but the design uncertainties are much larger for the C<sub>3</sub> Splitter. Qualitatively, this is an expected result. However the value of the MUM framework is that the design uncertainties can be quantified with modest effort.

### Case Study 3: Separation of the Benzene + Chloroform + Acetone System

This case study applies the MUM framework to the “textbook” separation of the acetone + chloroform + benzene system. The detailed analysis has been presented by Mathias,<sup>37</sup> and here we just summarize the key results. The example was proposed by Westerberg and Wahnschafft<sup>38</sup> as part of an extensive “tutorial on recent advances in the synthesis of ideal and nonideal distillation-based separation processes,” and used residue-curve analysis<sup>39,40</sup> to synthesize separation schemes for this ternary mixture. They proposed a two-column design and three-column alternatives. Mathias<sup>37</sup> limited his analysis to the two-column case (Figure 10) as the simplest case highlighted the key elements and benefits of the MUM framework. The feed to the process is a 100 kmol/h liquid mixture at 1 atm and its bubble-point temperature, containing 36 mol% acetone, 24 mol% chloroform and 40 mol% benzene. The feed is mixed with a chosen flow of recycle (stream REC) from the bottoms of the second column (Column 2), and fed to the first column (Column 1) in which high-purity acetone is obtained as distillate, and an essentially acetone-free mixture of chloroform and benzene is taken as the bottoms product. Column 2 produces high-purity chloroform as the distillate and high-purity benzene as the bottoms product. Both columns operate at a pressure of 1 atm, and pressure drops are assumed to be negligible. The design parameters and specifications are presented in Table 2.

**Table 2. Summary of design parameters and specifications for two-column flowsheet for the separation of the acetone – chloroform + benzene mixture. Both columns have a total condenser and a partial reboiler. Figure reprinted with permission from ref 37. Copyright 2016 Elsevier.**

Parameter	Column 1	Column 2
Number of stages	68	60
Feed stage (from top)	26	30
Distillate Rate (kmol/h)	36	24
Distillate design specification	Acetone mole fraction in distillate = 0.99	Chloroform mole fraction in distillate = 0.98
Variable to achieve design specification	Reflux ratio	Reflux ratio

The recycle flow rate (stream REC in the flowsheet, Figure 10) is considered to be an independent variable, and for each specification of the flow rate of stream REC, the reflux ratios, and hence the reboiler duties, in the two columns are calculated to achieve their respective design specifications. Here the sum of the two reboiler duties is taken as indicative of the operating cost, and hence the simulation enables a quantitative relationship between the operating cost and the recycle rate.

Mathias<sup>37</sup> performed extensive analysis of the VLE data for the three binary mixtures and the ternary mixture (some of these analyses have been presented earlier in this paper), and concluded that

uncertainty in the model K-values is  $\pm 5\%$ . The range of  $\delta$  values that results in a  $\pm 5\%$  perturbation in infinite-dilution activity coefficients is between 0.1 and 0.2. In order to perform the uncertainty analysis, the perturbation parameters need to be related to the phase-equilibrium uncertainties. As in the previous case study (Dehexanizer Column), in order to be conservative,  $\delta$  should be negative (i.e., lower the K-value) when the component is a light, and  $\delta$  should be positive when the component is a heavy. In Column 1, acetone is a light, while chloroform and benzene are heavies, while in Column 2, acetone and chloroform are lights and benzene is the heavy. To control the several perturbations with a single parameter, a perturbation scheme has been set up as follows:

$$\text{Column 1: } \delta_A = -\delta_0, \quad \delta_C = \delta_0, \quad \delta_B = \delta_0 \quad (7)$$

$$\text{Column 2: } \delta_A = -\delta_0, \quad \delta_C = -\delta_0, \quad \delta_B = \delta_0 \quad (8)$$

where the subscripts A, C and B refer to acetone, chloroform and benzene, respectively, and  $\delta_0$  is the single perturbation parameter. We note that the two separate perturbations in eq 7 and eq 8 have been implemented in Aspen Plus using the “multiple dataset” capability.<sup>41</sup>

The ternary residue curve (Figure 11) enables fundamental understanding of the separation process. There is one distillation boundary that divides the ternary diagram into two separate regions, and this distillation curve starts at pure benzene and ends at the acetone-chloroform azeotrope (about 65 mol % chloroform). The distillation boundary is curved, and stays at low concentration in acetone for the initial portion as it moves away from pure benzene. By mass balance, the two products of a distillation column with a feed to the left of the distillation boundary fall on a straight line that goes through the feed composition and, at most, ends on the distillation boundary, and it is desired that the distillate (D1) has 99 mol% acetone. With zero flow in REC it can be seen that the bottoms from Column 1 (dotted line in Figure 11) will have too high a concentration of acetone, and this renders the composition specification on Column 2 impossible to achieve (Table 2). A certain minimum flow of REC is needed to attain the three product specifications, and the reboiler duties generally rise with an increase in REC flow because the vapor and liquid flows in the two distillation columns will increase. These results follow from residue-curve analysis available in the literature. The goal of the present analysis is to evaluate what extra insights can be gleaned from the MUM framework.

Figure 12 presents the percentage increase in total reboiler duty as the perturbation parameter  $\delta_0$  (see eqs 7 and 8) is increased. The reference case is a recycle flow rate of 50 kmol/h and  $\delta_0 = 0$ . The solid circles represent the value of  $\delta_0$  beyond which the purity specifications cannot be met. The way to

understand this is to notice that increased values of  $\delta_0$  move the distillation boundary to the left; for example, see the dashed line in Figure 11. Thus each value of  $\delta_0$  has a minimum recycle rate; for example, for  $\delta_0 = 0.2$  a recycle rate of 50 kmol/h is inadequate and needs to be raised to 55 kmol/h. Hence, as the K-value uncertainty increases, the reboiler duty goes up in a nonlinear fashion because the separation becomes more difficult (required more reflux and hence higher reboiler duties), but also because the recycle rate needs to be increased. For the purposes of illustration, the increase of reboiler duty at K-value uncertainties of 5 %, 10 % and 15 % are shown, but it is noted that data analysis has determined that the model uncertainty is 5 % (about three standard deviations). Thanks to the strong database, the uncertainty in reboiler duty is quite small (about 12 %). However, if the model uncertainty were 15 %, the uncertainty in reboiler duty would rise to 50 %.

The value of the MUM framework is that the design uncertainty can be quantitatively estimated. If the design uncertainty is deemed to be too large, better data needs to be measured and/or a better activity-coefficient model developed.

#### **Case Study 4: Separation of the Water + 1-Butanol System**

Separation of the water + 1-butanol system is complex because this binary exhibits liquid-liquid equilibrium and forms a minimum-boiling heterogeneous azeotrope, and the typical separation scheme includes a decanter as well as two distillation columns. In addition, the NRTL model is unable to correlate the data within measurement uncertainty over a wide range of conditions, and hence a “local fit” was made limited to the conditions expected in this specific process.<sup>42</sup>

The separation process operates at atmospheric pressure and the temperatures of interest are in the range 360 to 390 K. The NRTL fit was limited to data over this temperature range. Figure 13 compares the NRTL fit to the reference correlation of Maczynski et al.<sup>43</sup> for liquid-liquid equilibrium. The fit is adequate in the 360-390 K temperature range, however the NRTL model is clearly inaccurate at lower and higher temperatures. Mathias<sup>42</sup> provides details of the model accuracy in the VLE regions, and these are not repeated here. The VLE fits at atmospheric pressure are quite good. It also turns out that the relative volatilities are quite high. In the water-rich region the infinite-dilution butanol-water relative volatility is about 30, while in the butanol-rich region, the water-butanol relative volatility is about 10.

The main products of fermentation processes that produce butanol are acetone, ethanol and 1-butanol, and a common separation scheme<sup>44</sup> to purify these products is shown in Figure 14. The specifications for the two columns in the flowsheet are presented in Figure 15 and Table 3. The feed contains 20 mol

% or 50.7 wt % 1-butanol. As in the previous example (Case Study 3), the activity-coefficient perturbations in the decanter and the two columns have been linked to a single perturbation parameter  $\delta_0$  (see Figure 15).

**Table 3. Specifications for water column (WA-COL) and 1-butanol column (BOH-COL). See Figure 15. Figure reprinted with permission from ref 42. Copyright 2016 ACS.**

Parameter	WA-COL	BOH-COL
Number of stages	5	10
Pressure /kPa	101.325	101.325
Specifications	Water purity of 99 wt%, 99.9 wt% and 99.99 wt%	1-butanol purity of 99.9 wt%
Vary variable	Reboiler duty	Reboiler duty

Figure 16 shows the change in total reboiler duty (both columns in Table 3) as a function of the perturbation parameter  $\delta_0$  for three values of the water purity from column WA-COL. Note that negative values of  $\delta_0$  are conservative. The change in total reboiler duty is relative to 99 wt% water from WA-COL and  $\delta_0 = 0$ . A perturbation of  $\delta_0 = -1$ , which is considered to be three standard deviations, causes an increase in total reboiler duty of only 12 %, which is remarkably low. Even though the NRTL model cannot provide a global good fit for this complex VLE binary mixture, a local fit that covers the region of interest enables a design with low uncertainty. Figure 16 also shows of increasing the water purity to 99.9 wt % and 99.99 wt %. There is, of course, an increase in reboiler duty for the base case ( $\delta_0 = 0$ ), but the curves remain almost parallel, indicating that the relative uncertainty is only weakly dependent on the product purity, which is in sharp contrast to the C<sub>3</sub> Splitter (Case Study 1), and results because the relative volatilities increase from about 1.1 to values greater than 10.

It is interesting and useful to quantitatively understand the contributions of the three process units to the increase in total reboiler duty, and these results are presented in Figure 17. The contribution from the water column (WA-COL) is relatively small, and the contributions from the other two units are approximately equal. As expected, the contribution from WA-COL increases from 11 % to 26 % as the water purity in stream PROD-WA increases from 99 wt % to 99 wt %. The benefit of the MUM framework is that these subtle details can be quantified, and the design engineer will be able to focus additional measurements or model improvements on specific areas of the process, e.g., a more targeted fit of the LLE (Figure 13) or more accurate VLE data in the butanol-rich region.

## Case Study 5: Effect of Phase-Equilibrium Uncertainties on Ethyl Acetate Purification

Mathias and Kister<sup>45</sup> applied the MUM framework to the purification of ethyl acetate from a ternary mixture with water and ethanol. This purification step occurs in the production of ethyl acetate via esterification of acetic acid with ethanol and has been practiced for many decades.<sup>46</sup> The study presented here follows the flowsheet and design of Tang, Huang and Chien,<sup>47</sup> but simplifies the modeling of the reactive-distillation column in order to focus on the purification of ethyl acetate from the ethyl acetate + ethanol + water ternary mixture.

The simplified flowsheet for ethyl acetate production used for the present analysis is shown in Figure 18, and the description of the various units has been described in the original paper.

Figure 19 presents the ternary map for the ethyl acetate + ethanol + water system at 101.3 kPa, and also shows key compositions in the process model. It is clear that the compositions of interest are at low ethanol concentrations, less than 5 mol%.

A thorough analysis of the VLE data for the three binaries and the ternary mixture has been reported by Mathias and Kister.<sup>45</sup> One point that should be emphasized is that commercial simulators such as Aspen Plus provide binary parameters for activity-coefficient models such as NRTL, but these parameters may not provide accurate results for particular ternary mixtures. Figure 20 compares the present model calculations<sup>45</sup> (circles) and calculations from the out-of-the-box Aspen Plus model (diamonds) to the data of Lee, Chen and Huang.<sup>48</sup> The out-of-the box Aspen Plus parameters provide a good prediction of the water + ethyl acetate LLE, but are inaccurate for the change in LLE as ethanol is added. The present NRTL fit is better since the binary parameters have been fit to ternary data in addition to the binary data. The conclusion is analogous to the one made for the water + 1-butanol system, namely that models such as NRTL are inadequate as “universal models” and therefore that local fits are necessary for specific engineering applications. In the water + 1-butanol system, the fit needed to be restricted to the temperature range of the application (360 – 390 K), while here the binary parameters are only valid for this particular ternary system.

The first study that was done investigated the effect of water feed rate (Figure 18) using the base models (Figure 20), and the results are presented in Figure 21. As noted by Tang et al.,<sup>47</sup> increased water flow reduces the stripper duty but also increases ethyl acetate losses. However, Figure 21 also demonstrates the adverse effect of an inaccurate multicomponent activity-coefficient model. For example, at a water flow rate of 10 mol/s, the reboiler duty can be underpredicted by 50 %. It is thus extremely important to use ternary data in the parameter estimation.

We now attempt to relate the VLE uncertainties in the stripper to a single “universal” perturbation parameter,”  $\delta_0$ , in the Margules perturbation framework.

$$\delta_{VLE-Water} = -\delta_0 \quad (9)$$

$$\delta_{VLE-Ethanol} = -\delta_0 \quad (10)$$

The negative sign of in eqs 9 and 10 ensures a conservative perturbation (decreased activity coefficients) for positive values of  $\delta_0$ . The detailed analysis of the VLE data performed by Mathias and Kister<sup>45</sup> concluded that a value of  $\delta_0 = 0.15$  represented three standard deviations. Figure 22 shows the effect of  $\delta_0$  on the reboiler duty. When the feed water flow is 18 mol/s, a perturbation of  $\delta_0 = 0.15$  (three standard deviations) increases the reboiler duty by 28 %, and this may be considered to be the uncertainty in the reboiler duty. As the feed water flow rate decreases, both reboiler duty and the sensitivity of the reboiler duty to phase-equilibrium uncertainty increase. For example, when the water flow is reduced to 10 mol/s, the base reboiler duty (no perturbation) rises by 56 % compared to 18 mol/s, and the effect of the perturbation is an additional 43 %.

The analyses presented in this case study are similar to those of the previous one. Careful attention needs to be devoted to data fitting and a “local fit” may be necessary. The MUM framework enables quantification of the propagation of phase-equilibrium uncertainties into variability of the design.

### Case Study 6: Trapping of Intermediate Components in Distillation

The issue of intermediate components in distillation is a subset of a general problem of component trapping that has been discussed extensively by Kister.<sup>49,50</sup> Intermediate components tend to accumulate near the middle of a distillation column in many chemical and petroleum separations. Their accumulation may lead to off-spec products, corrosion, plugging, or periodic cycling. The most common method of removing these intermediate components is by taking them out in one or more side draws. The addition of such side draws may not go far enough to achieve the desired product specs. If the side-draw approach fails, a multiple-column solution may be required. The multiple-column solution is the safe solution, but costs more than the single column with a side draw in terms of both capital and operating costs. Mathias et al.<sup>51</sup> quantified the risk of purifying an aqueous solution of acetonitrile (ACN) in a single column by using the MUM framework.

The objective was to purify an aqueous of 12 wt% ACN by distillation at atmospheric pressure, and to recover about 90 % of the ACN at the azeotropic composition, about 83 wt %. The separation is difficult due to the intermediate components Propionitrile (PPN) and t-crotonaldehyde (T-CROTON) that tend to accumulate in the distillation column.

The feed mixture studied by Mathias et al.<sup>51</sup> consisted of 14 components, including water, ACN, PPN and T-CROTON. The remaining 10 compounds were either heavies or lights, and therefore easy to

model. The water + ACN binary is well studied and is accurately modeled by the NRTL-RK property option. Hence the systems of interest are PPN and T-CROTON at low concentrations in ACN + water mixtures. This study focused on T-CROTON as the intermediate component of interest, with the expectation that the broad conclusions will also apply to PPN.

Figure 23 presents comparisons between model and data<sup>52</sup> for the K-value of T-CROTON at low concentration (effectively infinite dilution) in the water + ACN binary mixture at 1 atm (101.3 kPa). The dashed lines indicate  $\pm 30\%$  from the model calculations, and the dotted lines show perturbed model calculations with  $\delta=0.5$  and  $\delta=-0.5$ . Most of the data points fall within the dashed lines, and this may be considered to be the 99% uncertainty (about 2.6 standard deviations) of the model K-values for T-CROTON. The dotted lines (perturbed model) are equivalent to the  $\pm 30\%$  lines at the water-rich end, but have a smaller variation at the ACN-rich end. Based upon studying the uncertainties in Figure 23, we conclude that perturbations of  $\delta = \pm 0.5$  represent an expanded combined uncertainty (two standard deviations or 95% probability) in the T-CROTON K-value. It should be noted that these uncertainty estimates have some element of subjectivity, due to Type B uncertainties; Chirico et al.<sup>53</sup> define these Type B uncertainties as “evaluated by scientific judgment based upon all available information.” The vertical line in Figure 3 at 83 wt% shows the ACN + water azeotrope, which corresponds to the distillate composition from the column, and it is clear that both the model and experimental data indicate that the K-value of T-CROTON drops below unity before reaching the top of the column, which, of course, is the reason that T-CROTON is an intermediate component.

It is useful from a practical engineering viewpoint to convert the perturbation in  $\delta$  to a confidence limit (*CL*). In the present case, we are only concerned about positive values of  $\delta$  because negative values will result in an optimistic lower calculated concentration of T-CROTON in the distillate. Assuming that the model fit of the data is unbiased,  $\delta = 0$  will give a *CL* of 50%. If we further assume that the distribution of  $\delta$  values follows a standard normal distribution, *CL* may be estimated as,

$$CL(\delta) \approx \frac{1}{\sqrt{2\pi}} \int_{-\infty}^{\delta} e^{-\frac{(\delta/\sigma_{\delta})^2}{2}} d\delta \quad (11)$$

where  $\sigma_{\delta}$  is the standard deviation of  $\delta$ , and its value is equal to 0.25 based upon the above analysis.

Table 4 presents values of *CL* for selected values of  $\delta$  obtained through a numerical approximation to eq 11 using eq 7.1.26 from Abramowitz and Stegun<sup>54</sup> for the error function.

**Table 4. Calculated values of the confidence limit (*CL*) for selected values of  $\delta$ . Note that  $\sigma_{\delta}=0.25$ . Figure reprinted with permission from ref 51. Copyright 2017 ACS.**

$\delta$	$\delta/\sigma_{\delta}$	<i>CL</i> / %
----------	--------------------------	---------------

0	0	50.0
0.1	0.4	65.5
0.2	0.8	78.8
0.3	1.2	88.5
0.4	1.6	94.5
0.5	2.0	97.7
0.6	2.4	99.2

Two sets of studies have been conducted to evaluate the effect of T-CROTON VLE uncertainty on the performance of a single column. Figure 24 depicts the single column with side draw used for the first set of design studies. The feed flow is 770 kg/h and is an aqueous mixture containing 12 wt% ACN, and with minor impurities. The impurity levels of PPN and T-CROTON in the feed are 100 ppmw (parts per million by weight) and 20 ppmw, respectively. The column has 35 theoretical stages including a reboiler and a total condenser.<sup>55</sup> The distillate-to-feed ratio is set at 0.13, which corresponds to  $\approx 91\%$  ACN recovery at the azeotropic composition. The calculated reflux ratio is varied to obtain a T-CROTON concentration in the distillate of 1 ppmw. The feed stage is varied from 12 to 24. The base case is the feed to stage 20, and for this case the calculated reflux ratio is 7.0. Figure 25 shows the vapor and liquid concentration profiles (weight fraction) for ACN, PPN and T-CROTON in the distillation column for the base case. The concentration of ACN rises with stages toward the condenser (here in decreasing stage number) and quickly reaches the water + ACN azeotropic concentration just a few stages above the feed stage. The concentration profiles of PPN and T-CROTON show the characteristics of intermediate components since they both have concentration peaks below the feed stage. Note that the concentration peak of T-CROTON is about three orders of magnitude above the distillate and bottoms concentrations. The distillate and bottoms concentrations of PPN and T-CROTON are both small since most of these two components are removed in the side draw. Mathias et al.<sup>51</sup> studied the effect of the side draw, and it was concluded that varying the side draw changes the amount of T-CROTON in the bottoms (because it changes the amount of T-CROTON removed in the side draw), but it only has a weak effect on the concentration of T-CROTON in the distillate. Since the main goal here is to reduce the concentration of T-CROTON in the distillate, the next study is done with no side draw.

Figure 26 presents the single column with no side draw used for the second set of design studies, and with the total number of stages increased from 35 to 40. Other design conditions are the same as in Figure 24. Figure 27 studies how the reflux ratio needs to be adjusted to attain the spec of 1 ppmw T-

CROTON in the distillate as the perturbation parameter of T-CROTON ( $\delta$ ) and the number of stages are varied. Increasing the number of rectification stages is helpful in reducing the required reflux ratio, and this can be seen from Figure 25 because the concentrations of PPN and T-CROTON decrease monotonically in the rectification section of the column, but the effect is relatively weak. On the other hand increasing  $\delta$  (increased activity coefficient and therefore K-value of T-CROTON) results in a strong increase in the required reflux ratio. Very large reflux ratios cause problems, for example requiring large-diameter columns and significant increases in reboiler duty, and are usually resisted in industrial process-design practice. Figure 25 also shows the confidence limits (CL) for each value of  $\delta$ . Note that the confidence that  $-\infty \leq \delta \leq 0.4$  is 95%.

Figure 28 presents the results of a study where the reflux ratio has been fixed at 10.0, and the perturbation parameter ( $\delta$ ) and the number of rectification stages are varied. Figure 28 shows that the concentration of T-CROTON in the distillate is a very strong function of the uncertainty in the VLE, specifically the T-CROTON K-value. As  $\delta$  increases not only does the concentration of T-CROTON in the distillate increase beyond the target value (1 ppmw), but it can also exceed the feed concentration (20 ppmw), in effect concentrating undesired impurities in the product!

The vertical lines in Figure 28 relate the VLE perturbation ( $\delta$ ) to the confidence limits. At the 50% confidence level ( $\delta = 0$ ; see Table 4), the spec of 1 ppmw T-Croton in the distillate is achieved even if just 15 rectification stages are used. At the 79% confidence level (0.8 standard deviations or  $\delta = 0.2$ ; see Table 4), it will be possible to attain the 1 ppmw T-CROTON spec if the number of rectification stages is increased slightly above 25. However, at the 95% confidence level (1.6 standard deviations or  $\delta = 0.4$ ) not only will it be impossible to attain the T-CROTON spec of 1 ppmw, but the T-CROTON concentration in the distillate will actually exceed the feed concentration – effectively concentrating the unwanted impurity in the product. Charts like Figure 28 are crucial to making rational design decisions.

The uncertainty analysis presented here clearly indicates that the single-column solution is the risky option, and also quantifies the risk in terms of confidence limits.

## Conclusions

The purpose of this paper is to briefly present the MUM framework and then demonstrate its many benefits through six case studies. Readers who wish to study the details are referred to the original five publications.<sup>24,37,42,45,51</sup> In summary, the insights and results that have been gained are:

1. It is most important to perform thorough analysis of the phase-equilibrium data. The availability of highly automated has diminished the familiarity of chemical engineers with the underlying property data, but the availability of property databases makes it relatively easy to access and evaluate data and property models.
2. Activity-coefficient models may not be able to provide a “universal” fit of the data. However, the water + 1-butanol study (# 3) demonstrates that a “local” fit will reduce the uncertainties to low values for specific applications.
3. While commercial simulators such as Aspen Plus usually provide good binary parameters, these parameters may need to be adjusted for multicomponent systems, as has been shown here for the ethyl acetate + water + ethanol ternary system. This may be considered to be another example of a “local” fit of the data.
4. The rough guideline presented by Fair<sup>22</sup> is useful as a first pass estimate because sensitivity to phase equilibrium grows exponentially as the relative volatility approaches unity. However, designs are also sensitive to product purity, as demonstrated for the C<sub>3</sub> Splitter (# 1), and thus is necessary to perform studies for all cases.
5. In many cases careful data fitting can reduce the design uncertainty to low values. This is the case for the Dehexanizer Column, however analysis needs to be done to quantify the sensitivity.
6. The acetone + chloroform + benzene case study (# 3) shows the relationship between residue-curve analysis and sensitivity studies. This example also demonstrates that uncertainties in properties may not affect process synthesis, but still need to be performed to quantify uncertainties in process design.
7. The MUM framework may be practically applied to systems containing a large number of components (Dehexanizer Column, # 2), in this case by assuming the two perturbation parameters, one for the lights and another for the heavies.
8. The purification of acetonitrile by distillation example demonstrates how the MUM framework may be applied to component trapping. This example demonstrates how the MUM framework may be used to quantify the confidence limit of the design.

It is our hope that this paper will encourage others to apply uncertainty analysis in their work and to invent new and improved frameworks and approaches to perform uncertainty analysis. Regardless of

improved methodologies, we are confident that data analysis will always remain the corner stone of uncertainty analysis.

## **List of Tables**

Table 1. Effect of Activity-Coefficient Perturbation on Dehexanizer Column design. Figure reprinted with permission from ref 24. Copyright 2014 ACS. ....	10
Table 2. Summary of design parameters and specifications for two-column flowsheet for the separation of the acetone – chloroform + benzene mixture. Both columns have a total condenser and a partial reboiler. Figure reprinted with permission from ref 37. Copyright 2016 Elsevier.....	11
Table 3. Specifications for water column (WA-COL) and 1-butanol column (BOH-COL). See Figure 15. Figure reprinted with permission from ref 42. Copyright 2016 ACS. ....	14
Table 4. Calculated values of the confidence limit ( <i>CL</i> ) for selected values of $\delta$ . Note that $\sigma_\delta = 0.25$ . Figure reprinted with permission from ref 51. Copyright 2017 ACS. ....	17

## **List of Figures**

Figure 1. The cost of inaccurate relative-volatility data on capital and operating cost. Estimates have been reported by Fair (see Table 8 of the paper) <sup>22</sup> for a 10 % error in activity coefficient.....	25
Figure 2. Percentage change in $\gamma^\infty$ calculated by eq 2 as a function of $\gamma^{\text{moo}}$ and at various values of $\delta$ . Figure reprinted with permission from ref 24. Copyright 2014 ACS. ....	26
Figure 3. Txy diagram of the acetone-chloroform binary mixture at 101.3 kPa. Comparison of model calculations to the data of Kojima et al. <sup>32</sup> Figure reprinted with permission from ref. 37. Copyright 2016 Elsevier. ....	27
Figure 4. Relative volatilities of the acetone + chloroform system at 101.3 kPa. Comparison of model results to the data of data of Kudryavtseva and Susarev, <sup>33</sup> Kogan and Diezenrot, <sup>34</sup> Kojima et al., <sup>32</sup> and Segura et al. <sup>35</sup> The chart also shows (dashed lines) $\pm 5\%$ deviations from the calculated relative volatility. Figure reprinted with permission from ref 37. Copyright 2016 Elsevier.....	28
Figure 5. Percentage errors of model K-values of acetone in comparison to the ternary VLE data of Reinders and de Minjer <sup>36</sup> and Kojima et al. <sup>32</sup> for the acetone + chloroform + benzene ternary mixture at 101.3 kPa. Figure reprinted with permission from ref 37. Copyright 2016 Elsevier. ....	29
Figure 6. Effect of changing the propylene:propane relative volatility at low concentrations of propylene on the calculated reboiler duty. The calculations have been done at four concentrations of propylene in the propane-rich product. Figure reprinted with permission from ref 24. Copyright 2014 ACS. ....	30
Figure 7. Effect of changing the peopylene:propane relative volatility at low concentrations of propane on the calculated reboiler duty. The calculations have been done at four concentrations of propane in the propylene-rich product. Figure reprinted with permission from ref 24. Copyright 2014 ACS.....	31
Figure 8. Component split to distillate in the Dehexanizer Column as a function of normal boiling point. The component codes are: 22DMB - 2,2-dimethylbutane, 23DMB - 2,3dimethylbutane, 2MP - 2-methylpentane, 3MP - 3-methylpentane, N-C6 – n-hexane, C6-OLIFN – trans-2-hexene, MCP – methylcyclopentane, BENZENE – benzene, 22DMP – 2,2-dimethylpentane, 24DMP – 2,4-dimethylpentane, CH – cyclohexane, 223TMB – 2,2,3-trimethylbutane, 33DMP – 3,3-dimethylpentane. The curve approximately follows the paraffins (except benzene).....	32

Figure 9. Activity coefficients of selected compounds in Dehexanizer Column as a function of stage number. The feed stage is # 23. The component codes have been given in Figure 8. Figure reprinted with permission from ref 24. Copyright 2014 ACS. ....	33
Figure 10. Two-column flowsheet for the separation of the acetone + chloroform + benzene ternary mixture. Figure reprinted with permission from ref 24. Copyright 2014 ACS. ....	34
Figure 11. Residue curve diagram for the acetone-chloroform-benzene ternary mixture at 1 atm. Three distillation boundaries are shown: Distillation Boundary-0 (thick black line) corresponds to the base case with the NRTL model, and all three perturbation parameters set to zero; Distillation Boundary-1 (dashed black line) has perturbation parameters $\delta_A=-0.2$ , $\delta_C=0.2$ , $\delta_B=0.2$ ; and Distillation Boundary-2 (double line) has perturbation parameters $\delta_A=-0.2$ , $\delta_C=-0.2$ , $\delta_B=0.2$ . The solid red lines show the feed (F), the combined feed to column 1 (F1), and the products from the flowsheet (D1, D2 and B2). The dotted line indicates the distillate and bottoms from COL1 if the recycle flow is zero. See Figure 10 for the flowsheet. Figure reprinted with permission from ref 37. Copyright 2016 Elsevier. ....	35
Figure 12. Effect of perturbation parameter, $\delta_0$ , on the percentage change in the total reboiler duty at various values of the recycle rate (in kmol/h). The solid circles represent the point beyond which the composition specifications cannot be attained each recycle flow rate. The double curve shows the results at an average uncertainty in component K-values. Figure reprinted with permission from ref 37. Copyright 2016 Elsevier. ....	36
Figure 13. Liquid-liquid equilibrium in the water + 1-butanol system. Comparison of the NRTL fit to the reference correlation of Maczynski et al. <sup>43</sup> Figure reprinted with permission from ref 42. Copyright 2016 ACS. ....	37
Figure 14. Separation train to produce acetone, ethanol and 1-butanol from fermentation broth. The highlighted section identifies the subsection studied in this paper. Figure reprinted with permission from ref 42. Copyright 2016 ACS. ....	38
Figure 15. Graphic explaining how the perturbations have been implemented in Aspen Plus. Three separate perturbations have been implemented through the universal perturbation parameter $\delta_0$ and the “multiple dataset capability” in Aspen Plus. <sup>41</sup> Figure reprinted with permission from ref 42. Copyright 2016 ACS. ....	39
Figure 16. Percentage change in total reboiler duties (sum of the reboiler duties in WA-COL and BOH-COL) as a function of the single perturbation variable $\delta_0$ . The base value is 99 wt% water in stream PROD-WA with no perturbation. Figure reprinted with permission from ref 42. Copyright 2016 ACS. ....	40
Figure 17. Relative contributions of the three process units (decanter and two distillation columns) to the increase in total reboiler duties as a function of purity of the water product in stream PROD-WA for a full perturbation ( $\delta_0 = 0$ ). Figure reprinted with permission from ref 42. Copyright 2016 ACS. ....	41
Figure 18. Aspen Plus flowsheet for ethyl acetate purification. Figure reprinted with permission from ref 45. Copyright 2017 ACS. ....	42
Figure 19. Ternary map of the ethyl acetate + ethanol + water system at 101.3 kPa. The double line shows the two-liquid phase boundary and the dashed lined within the dome present the tie lines. The four azeotropes are depicted by the large circles, and these identify the ends of the distillation boundaries, which divide the diagram into three regions. The small triangles show how the product from the reactive-distillation column (REACDIST) is changes after mixing with the distillate from the stripper (STRIPPER) and the water feed (WATER); this line must coincide with a tie line. The lines	

with the diamonds show how the feed to the stripper is separated into the product (PRODUCT) and the distillate (D-STRIP). Note that D-STRIP lies on a distillation boundary. Figure reprinted with permission from ref 45. Copyright 2017 ACS.....	43
Figure 20. Liquid-liquid equilibrium in the ethyl acetate + ethanol + water ternary system at 101.3 kPa. The present model calculations (circles) and calculations from the out-of-the-box Aspen Plus model (diamonds) are compared to the data of lee, Chen and Huang. <sup>48</sup> Figure reprinted with permission from ref 45. Copyright 2017 ACS.....	44
Figure 21. Effect of feed water flow on the stripper reboiler duty and the percentage ethyl acetate loss. The solid lines are results for the NRTL model developed here, while the dashed lines are for the NRTL parameters from the AspenTech database. Figure reprinted with permission from ref 45. Copyright 2017 ACS. ....	45
Figure 22. Effect of variation in the perturbation parameter ( $\delta_0$ ) on the stripper reboiler duty. See Figure 18 for flowsheet. Figure reprinted with permission from ref 45. Copyright 2017 ACS.....	46
Figure 23. Mass K-Value of T-CROTON at low concentration in water + ACN at 1 atm (101.3 kPa). Comparison of model calculations to Eli Lilly data. The dashed lines show $\pm 30\%$ from the model results. The dotted lines are model calculations with $\delta = 0.5$ and $\delta = -0.5$ . The vertical line indicates the water + ACN azeotrope. Figure reprinted with permission from ref 51. Copyright 2017 ACS. ....	47
Figure 24. Single column with side draw used for component-trapping perturbation studies-1. The column operates at 1 atm (101.3 kPa). Figure reprinted with permission from ref 51. Copyright 2017 ACS. ....	48
Figure 25. Vapor and liquid concentration profiles for ACN, PPN and T-CROTON in the distillation column corresponding to Figure 24, and with feed to stage 20. Figure reprinted with permission from ref 51. Copyright 2017 ACS.....	49
Figure 26. Single column used for component-trapping perturbation studies-2. The difference from Figure 24 is that the side draw has been eliminated. Figure reprinted with permission from ref 51. Copyright 2017 ACS. ....	50
Figure 27. Effect of perturbation parameter ( $\delta$ ) and number of rectification stages on the reflux ratio required to meet the spec of 1 ppmw T-CROTON in the distillate. See Figure 26 for details. The percentage in brackets show the extent of the perturbations at the ACN-rich and water-rich ends; the water-rich end has the larger perturbation. The confidence limits (CL) are also shown for each of the three values of $\delta$ . Figure reprinted with permission from ref 51. Copyright 2017 ACS.....	51
Figure 28. Effect of perturbation parameter ( $\delta$ ) and number of rectification stages on concentration of T-CROTON in distillate. Referring to Figure 26, the reflux ratio is fixed at 10. The vertical lines show the 79% and 95% confidence limits (CL); other values of CL may be estimated using Table 4. Figure reprinted with permission from ref 51. Copyright 2017 ACS.....	52

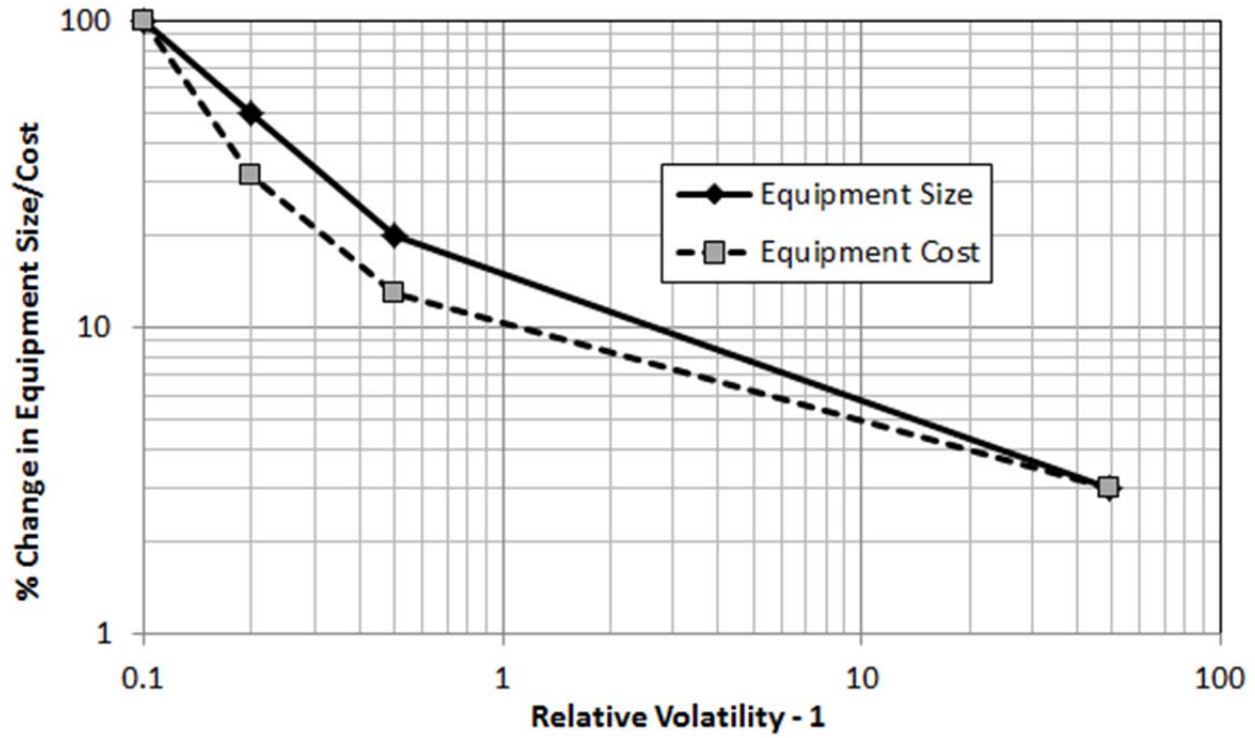


Figure 1. The cost of inaccurate relative-volatility data on capital and operating cost. Estimates have been reported by Fair (see Table 8 of the paper)<sup>22</sup> for a 10 % error in activity coefficient.

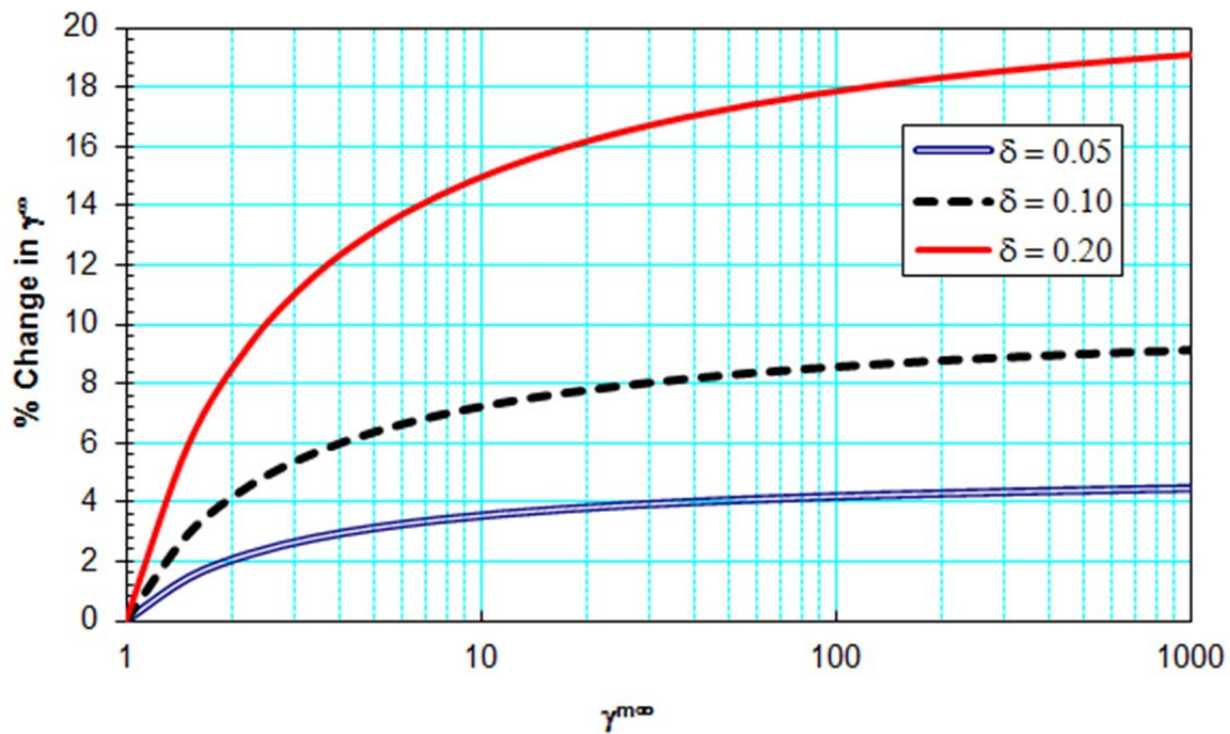


Figure 2. Percentage change in  $\gamma^\infty$  calculated by eq 2 as a function of  $\gamma^{m\infty}$  and at various values of  $\delta$ . Figure reprinted with permission from ref 24. Copyright 2014 ACS.

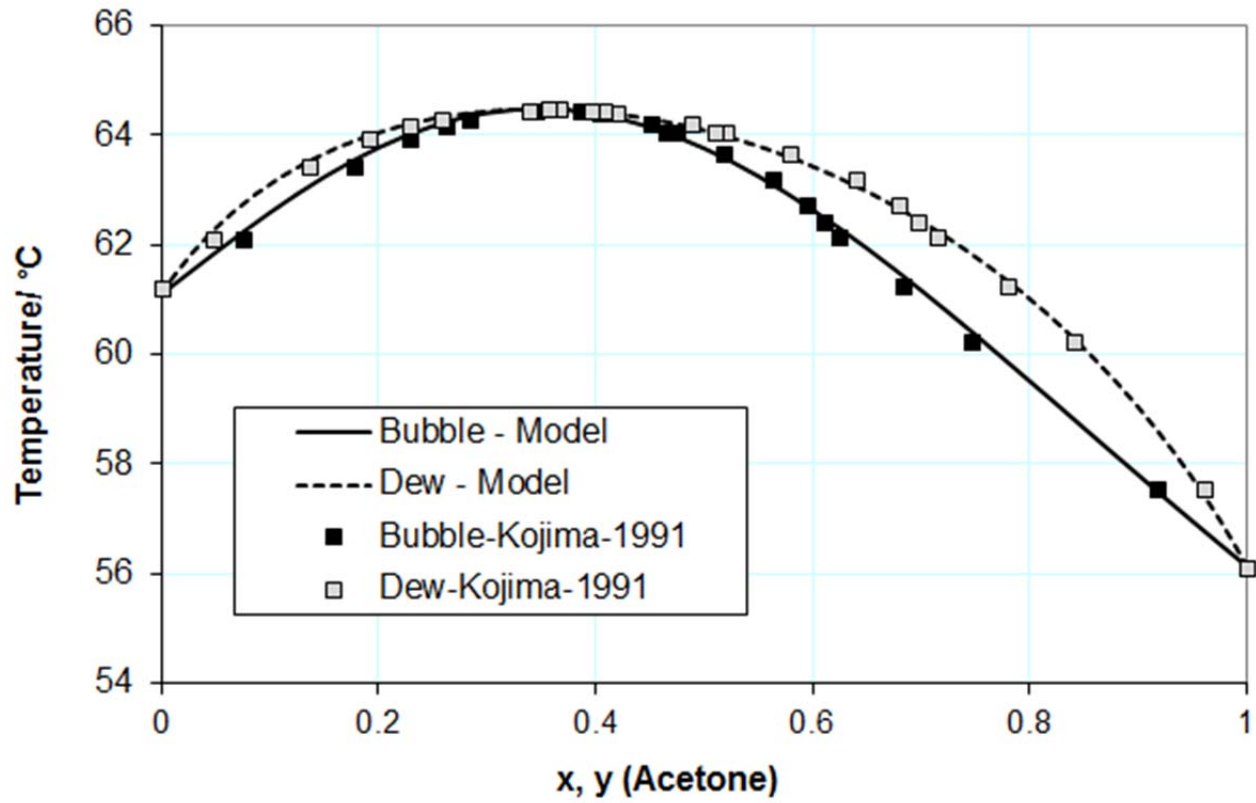


Figure 3. Txy diagram of the acetone-chloroform binary mixture at 101.3 kPa. Comparison of model calculations to the data of Kojima et al.<sup>32</sup> Figure reprinted with permission from ref. 37. Copyright 2016 Elsevier.

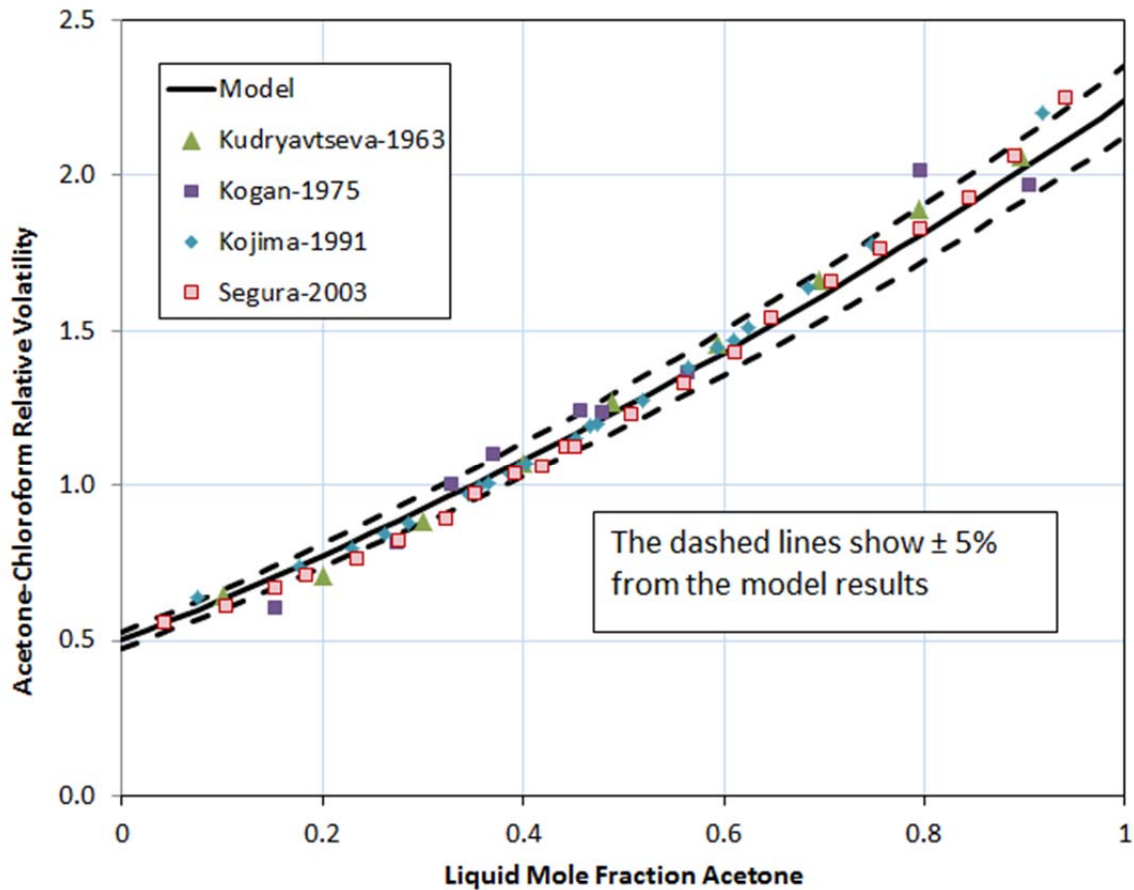


Figure 4. Relative volatilities of the acetone + chloroform system at 101.3 kPa. Comparison of model results to the data of data of Kudryavtseva and Susarev,<sup>33</sup> Kogan and Diezenrot,<sup>34</sup> Kojima et al.,<sup>32</sup> and Segura et al.<sup>35</sup> The chart also shows (dashed lines)  $\pm 5\%$  deviations from the calculated relative volatility. Figure reprinted with permission from ref 37. Copyright 2016 Elsevier.

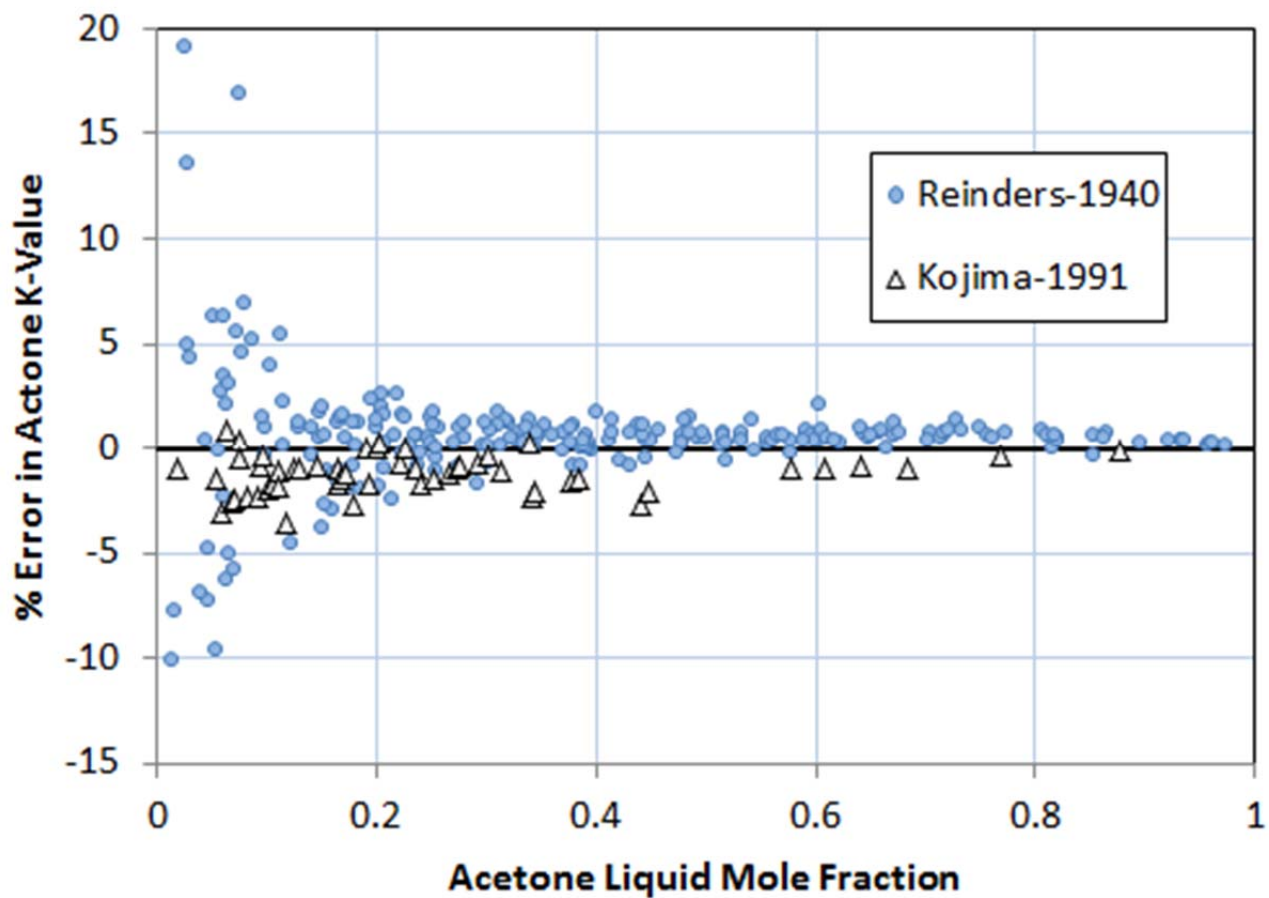


Figure 5. Percentage errors of model K-values of acetone in comparison to the ternary VLE data of Reinders and de Minjer<sup>36</sup> and Kojima et al.<sup>32</sup> for the acetone + chloroform + benzene ternary mixture at 101.3 kPa. Figure reprinted with permission from ref 37. Copyright 2016 Elsevier.

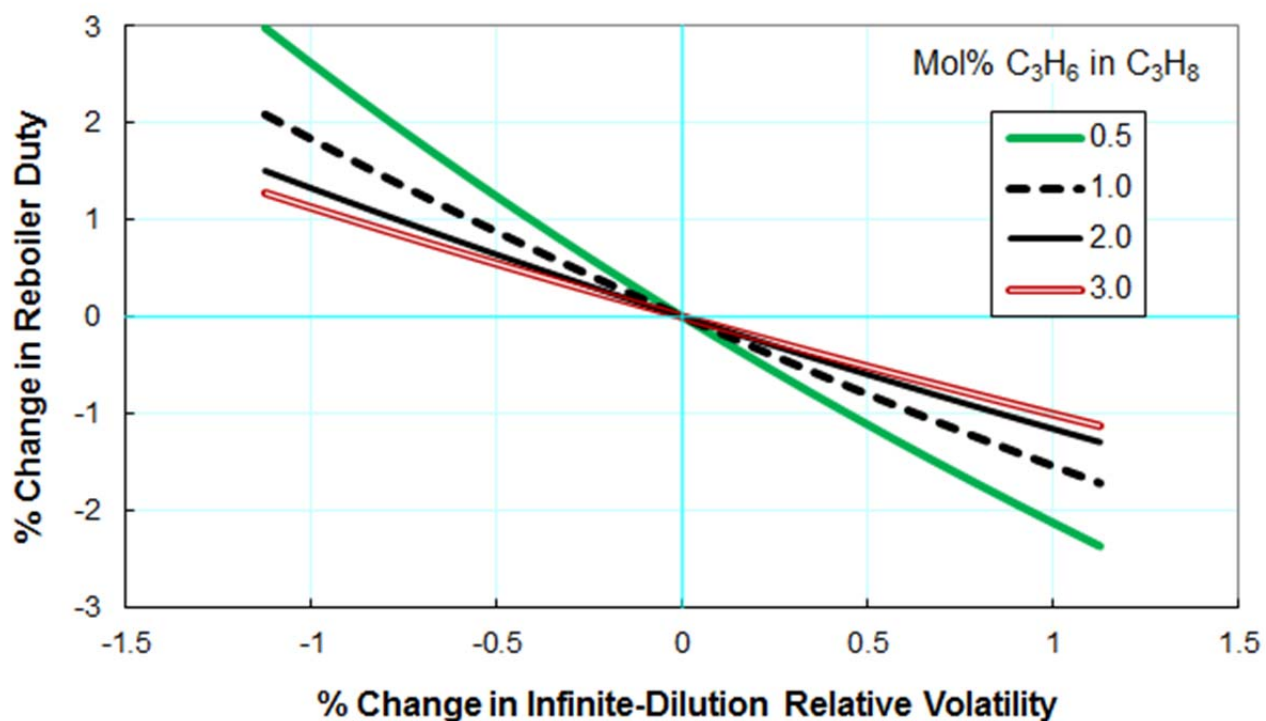


Figure 6. Effect of changing the propylene:propane relative volatility at low concentrations of propylene on the calculated reboiler duty. The calculations have been done at four concentrations of propylene in the propane-rich product. Figure reprinted with permission from ref 24. Copyright 2014 ACS.

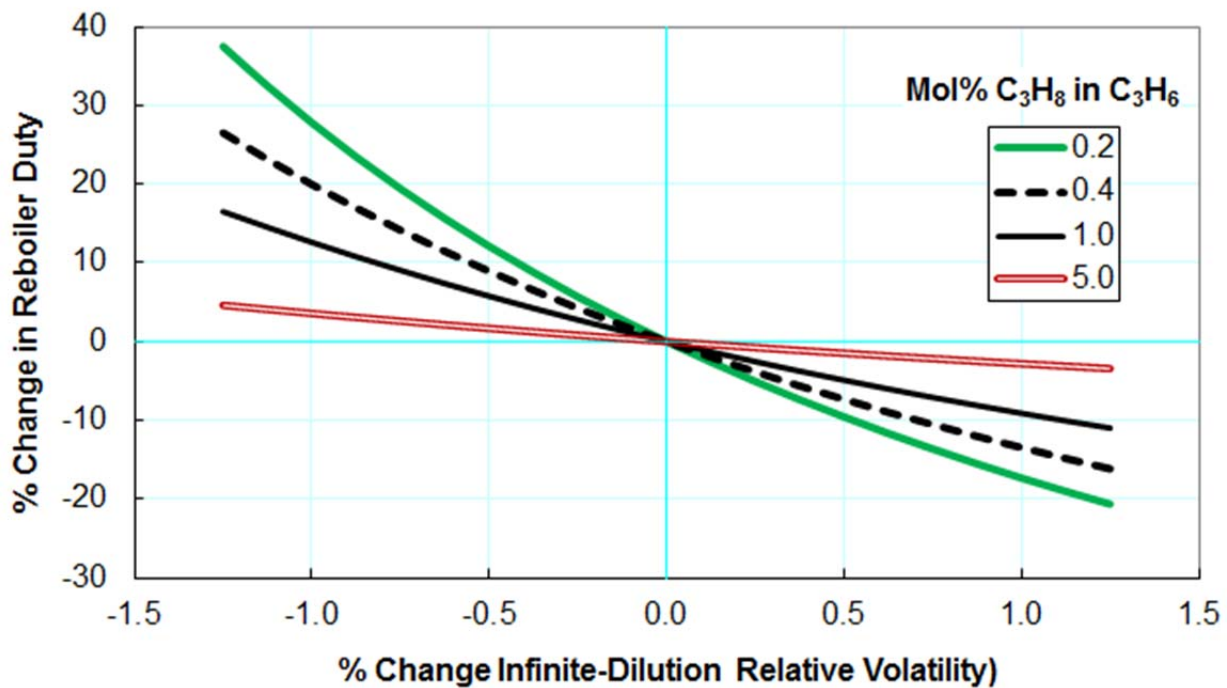


Figure 7. Effect of changing the propylene:propane relative volatility at low concentrations of propane on the calculated reboiler duty. The calculations have been done at four concentrations of propane in the propylene-rich product. Figure reprinted with permission from ref 24. Copyright 2014 ACS.

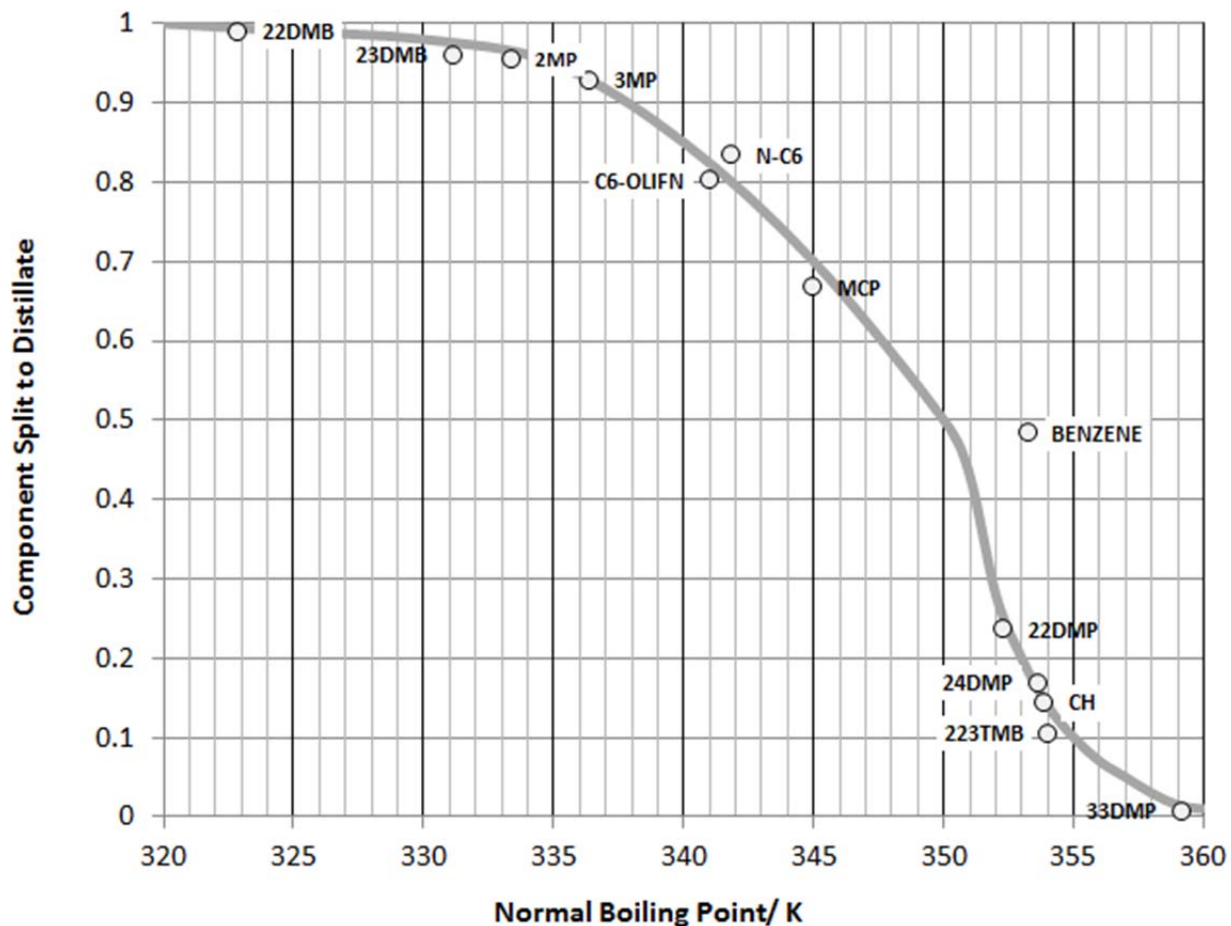


Figure 8. Component split to distillate in the Dehexanizer Column as a function of normal boiling point. The component codes are: 22DMB - 2,2-dimethylbutane, 23DMB - 2,3dimethylbutane, 2MP - 2-methylpentane, 3MP - 3-methylpentane, N-C6 - n-hexane, C6-OLIFN - trans-2-hexene, MCP - methylocyclopentane, BENZENE - benzene, 22DMP - 2,2-dimethylpentane, 24DMP - 2,4-dimethylpentane, CH - cyclohexane, 223TMB - 2,2,3-trimethylbutane, 33DMP - 3,3-dimethylpentane. The curve approximately follows the paraffins (except benzene).

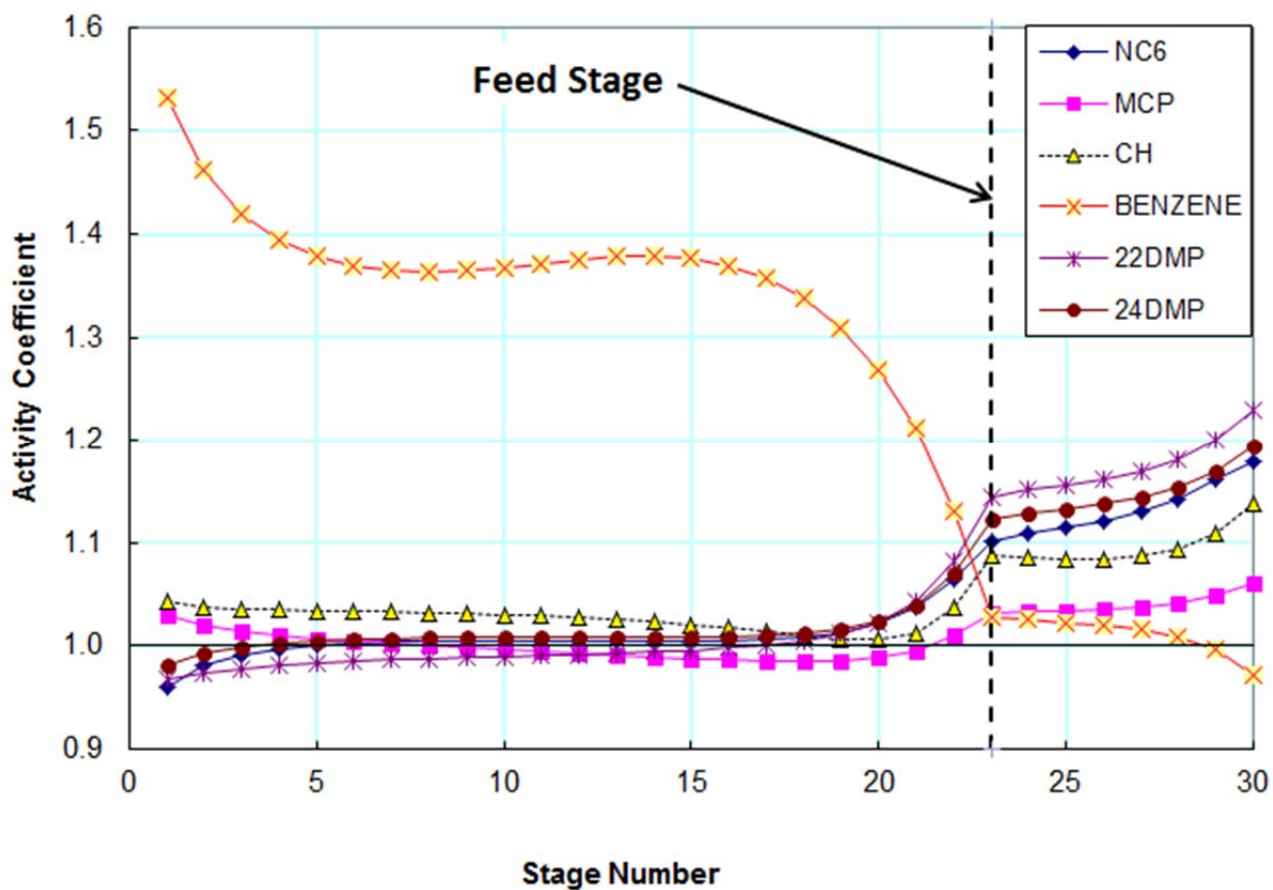
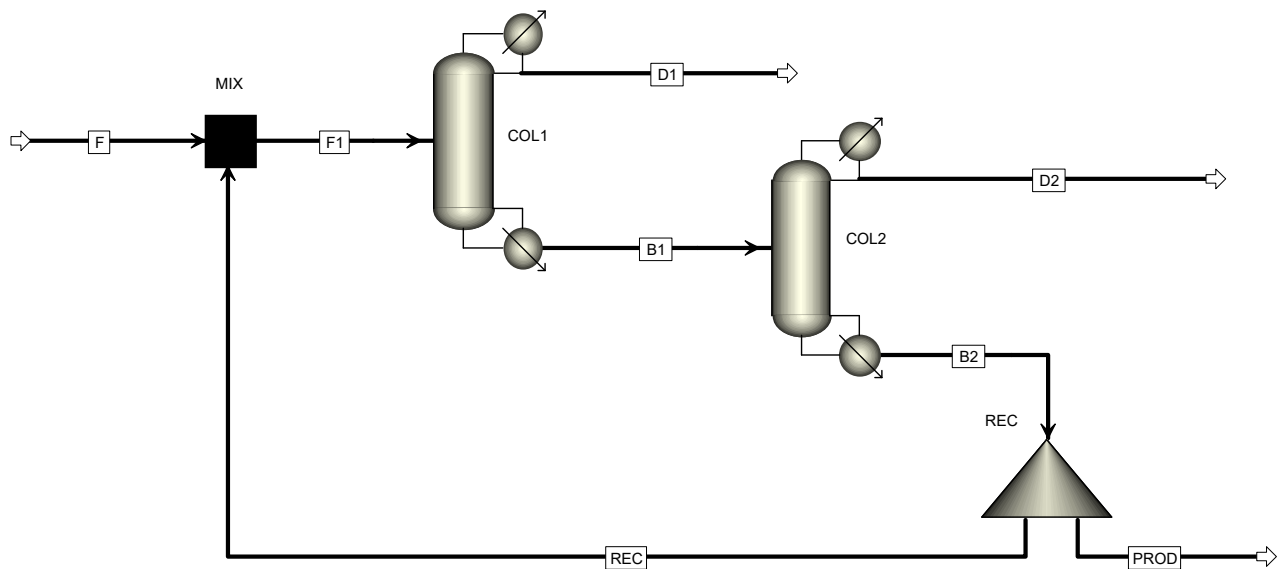


Figure 9. Activity coefficients of selected compounds in Dehexanizer Column as a function of stage number. The feed stage is # 23. The component codes have been given in Figure 8. Figure reprinted with permission from ref 24. Copyright 2014 ACS.



**Figure 10. Two-column flowsheet for the separation of the acetone + chloroform + benzene ternary mixture. Figure reprinted with permission from ref 24. Copyright 2014 ACS.**

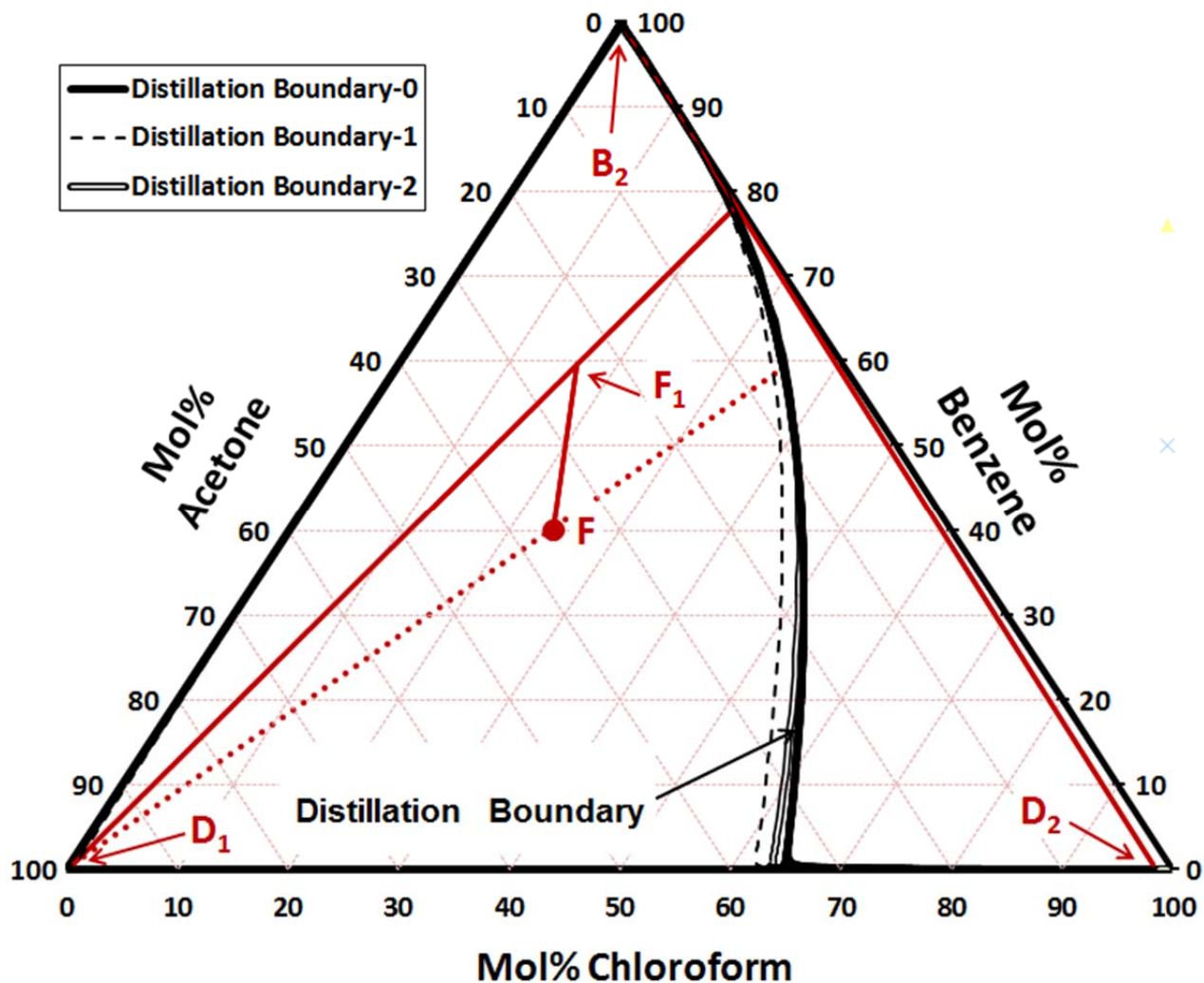


Figure 11. Residue curve diagram for the acetone-chloroform-benzene ternary mixture at 1 atm. Three distillation boundaries are shown: Distillation Boundary-0 (thick black line) corresponds to the base case with the NRTL model, and all three perturbation parameters set to zero; Distillation Boundary-1 (dashed black line) has perturbation parameters  $\delta_A=-0.2$ ,  $\delta_C=0.2$ ,  $\delta_B=0.2$ ; and Distillation Boundary-2 (double line) has perturbation parameters  $\delta_A=-0.2$ ,  $\delta_C=-0.2$ ,  $\delta_B=0.2$ . The solid red lines show the feed (F), the combined feed to column 1 (F1), and the products from the flowsheet (D1, D2 and B2). The dotted line indicates the distillate and bottoms from COL1 if the recycle flow is zero. See Figure 10 for the flowsheet. Figure reprinted with permission from ref 37. Copyright 2016 Elsevier.

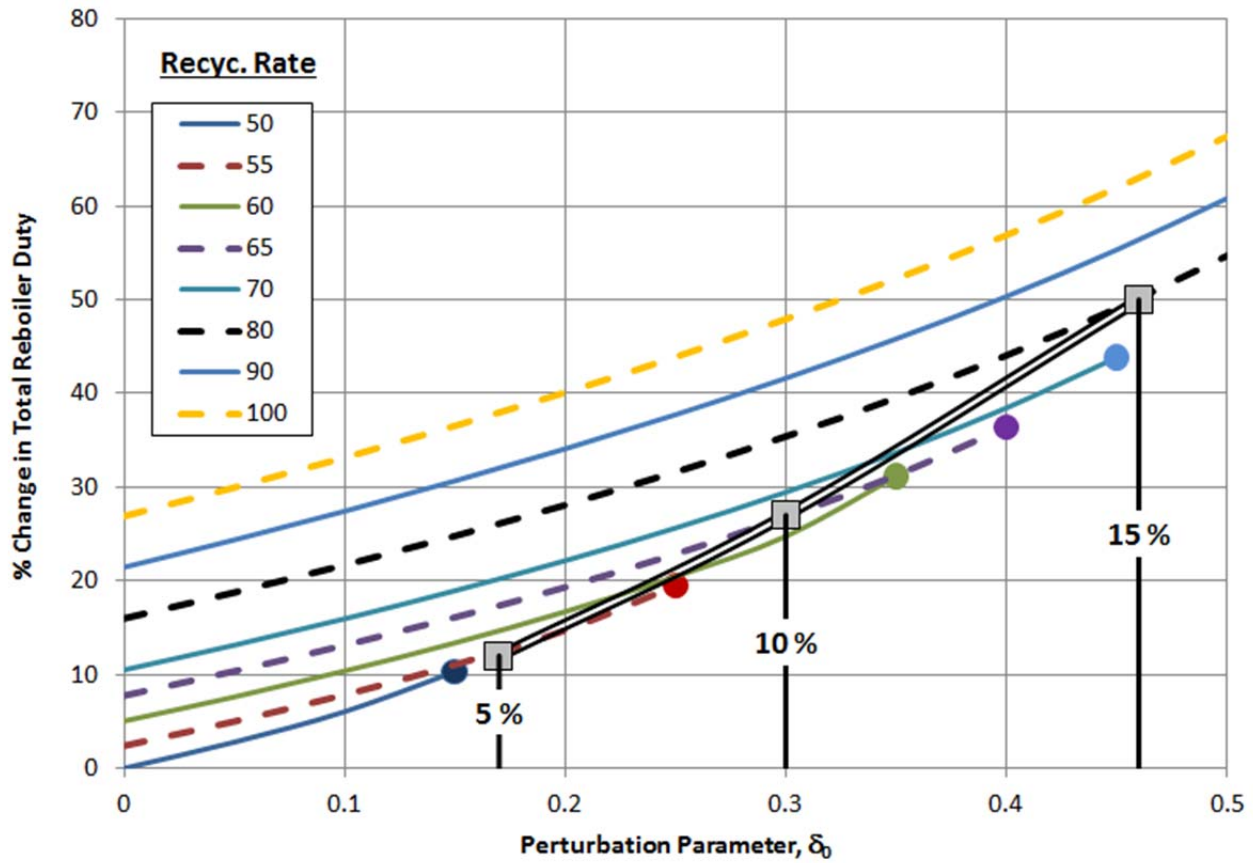


Figure 12. Effect of perturbation parameter,  $\delta_0$ , on the percentage change in the total reboiler duty at various values of the recycle rate (in kmol/h). The solid circles represent the point beyond which the composition specifications cannot be attained each recycle flow rate. The double curve shows the results at an average uncertainty in component K-values. Figure reprinted with permission from ref 37. Copyright 2016 Elsevier.

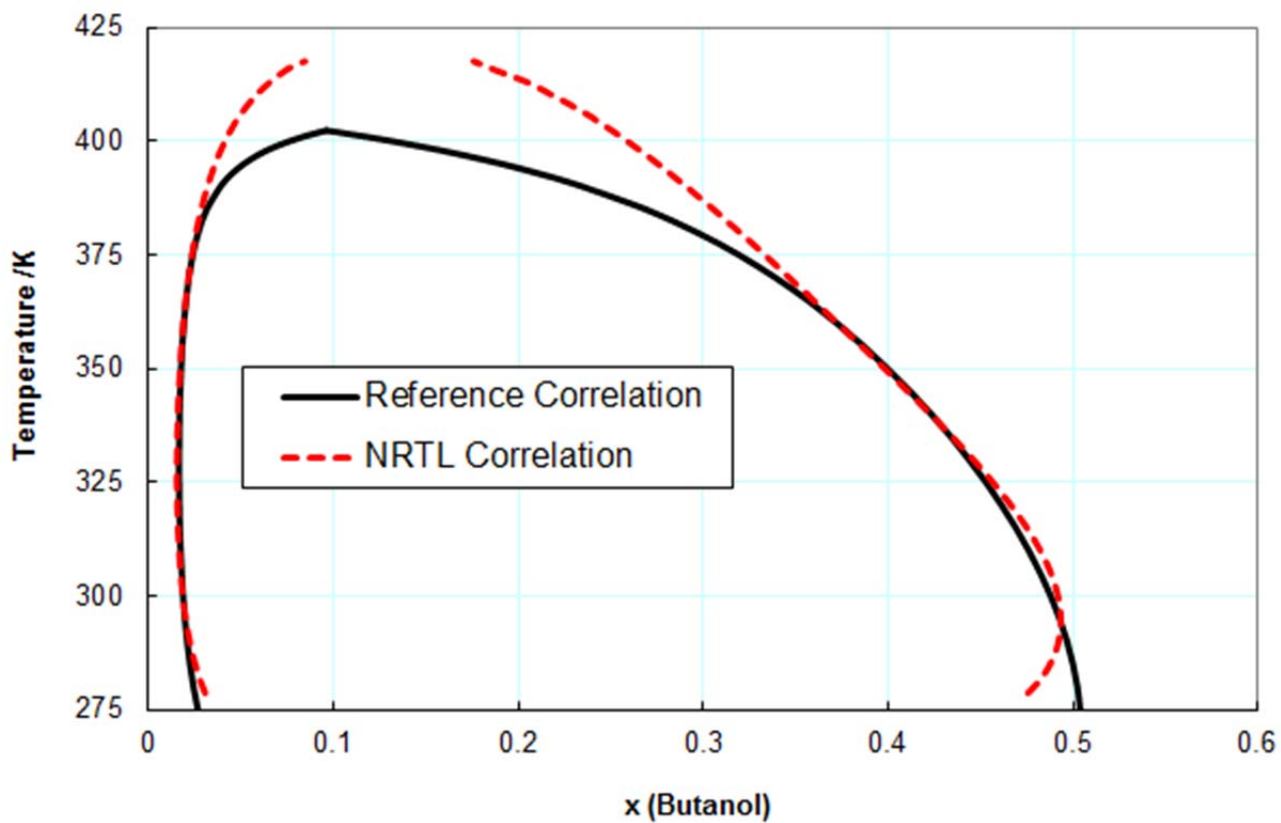


Figure 13. Liquid-liquid equilibrium in the water + 1-butanol system. Comparison of the NRTL fit to the reference correlation of Maczynski et al.<sup>43</sup> Figure reprinted with permission from ref 42. Copyright 2016 ACS.

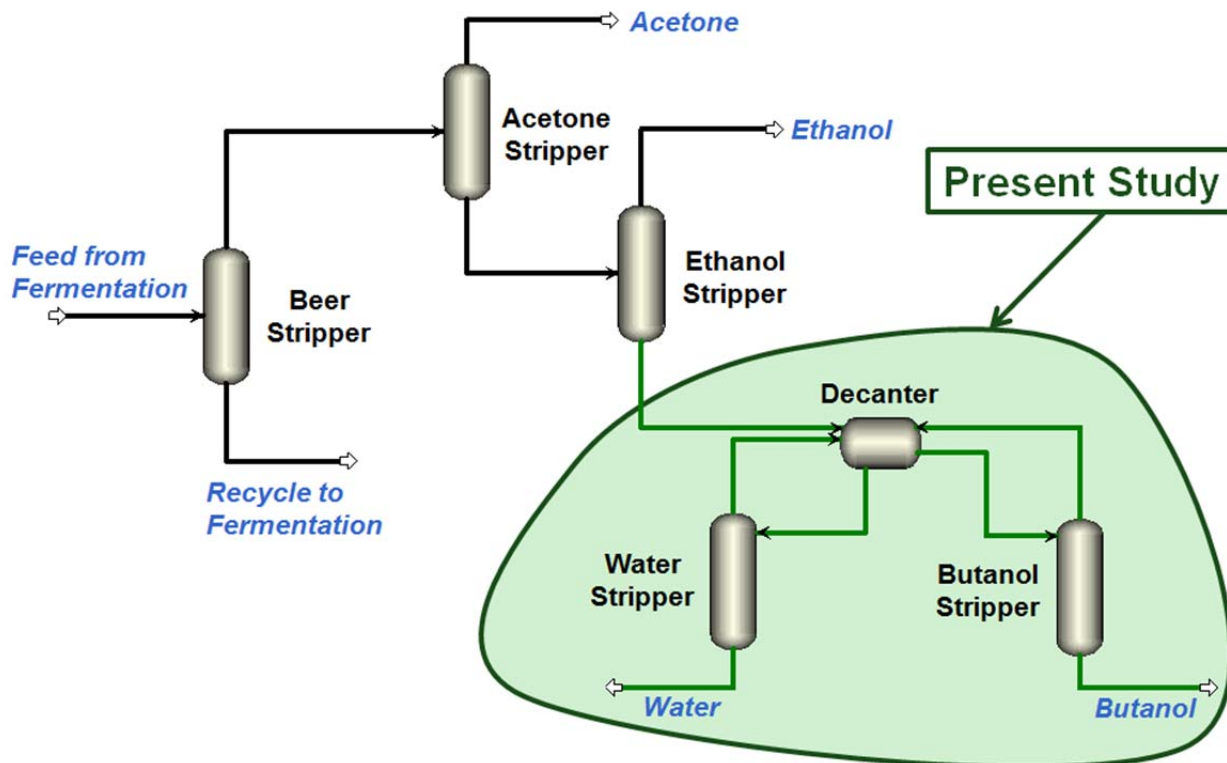


Figure 14. Separation train to produce acetone, ethanol and 1-butanol from fermentation broth. The highlighted section identifies the subsection studied in this paper. Figure reprinted with permission from ref 42. Copyright 2016 ACS.



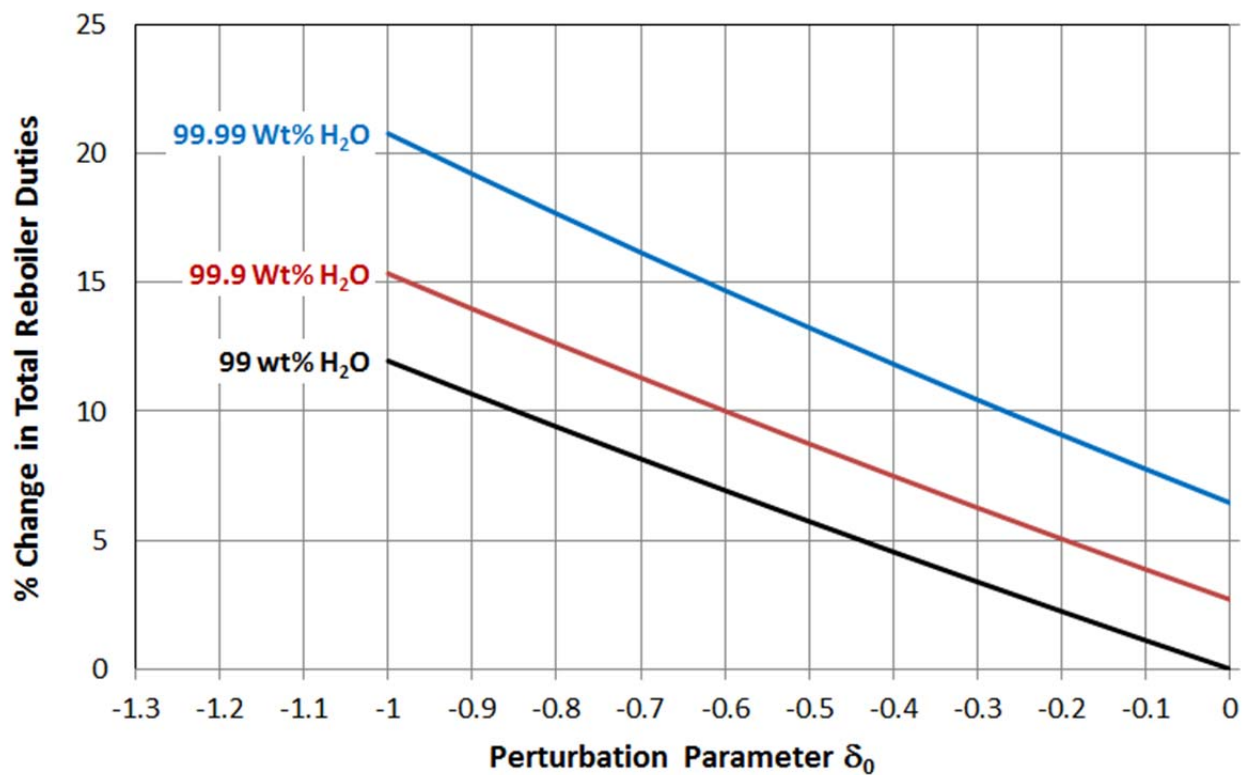


Figure 16. Percentage change in total reboiler duties (sum of the reboiler duties in WA-COL and BOH-COL) as a function of the single perturbation variable  $\delta_0$ . The base value is 99 wt% water in stream PROD-WA with no perturbation. Figure reprinted with permission from ref 42. Copyright 2016 ACS.

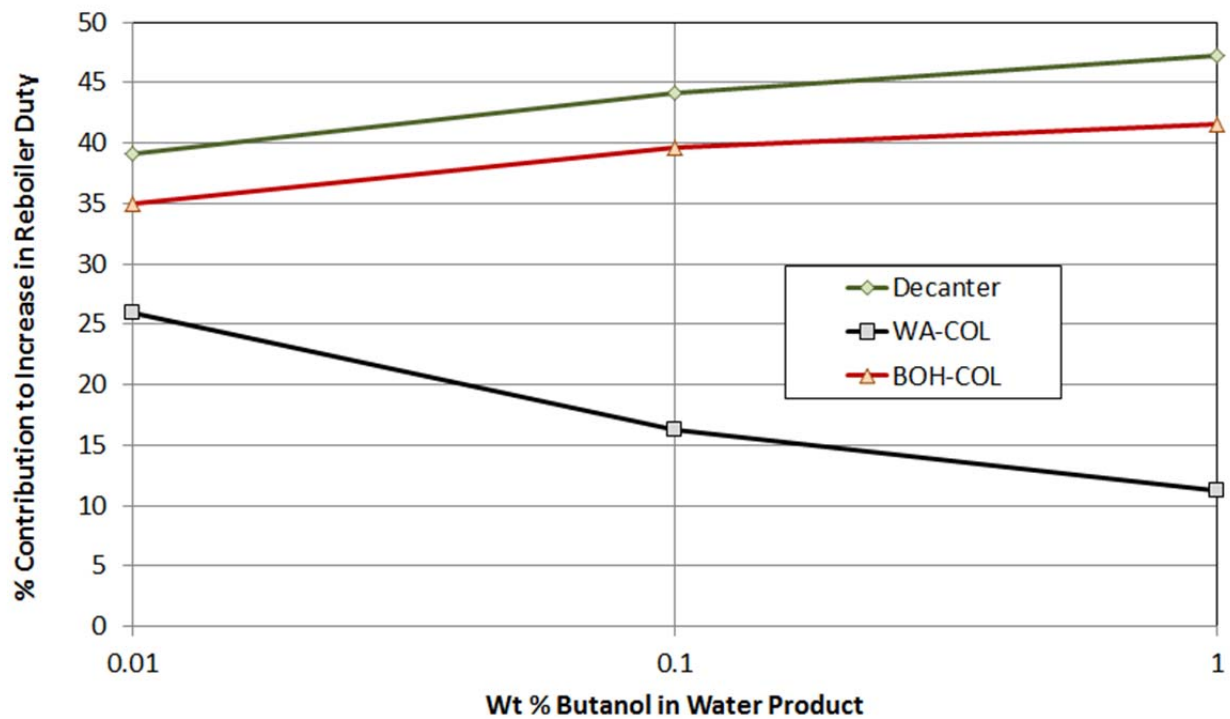


Figure 17. Relative contributions of the three process units (decanter and two distillation columns) to the increase in total reboiler duties as a function of purity of the water product in stream PROD-WA for a full perturbation ( $\delta_0 = 0$ ). Figure reprinted with permission from ref 42. Copyright 2016 ACS.

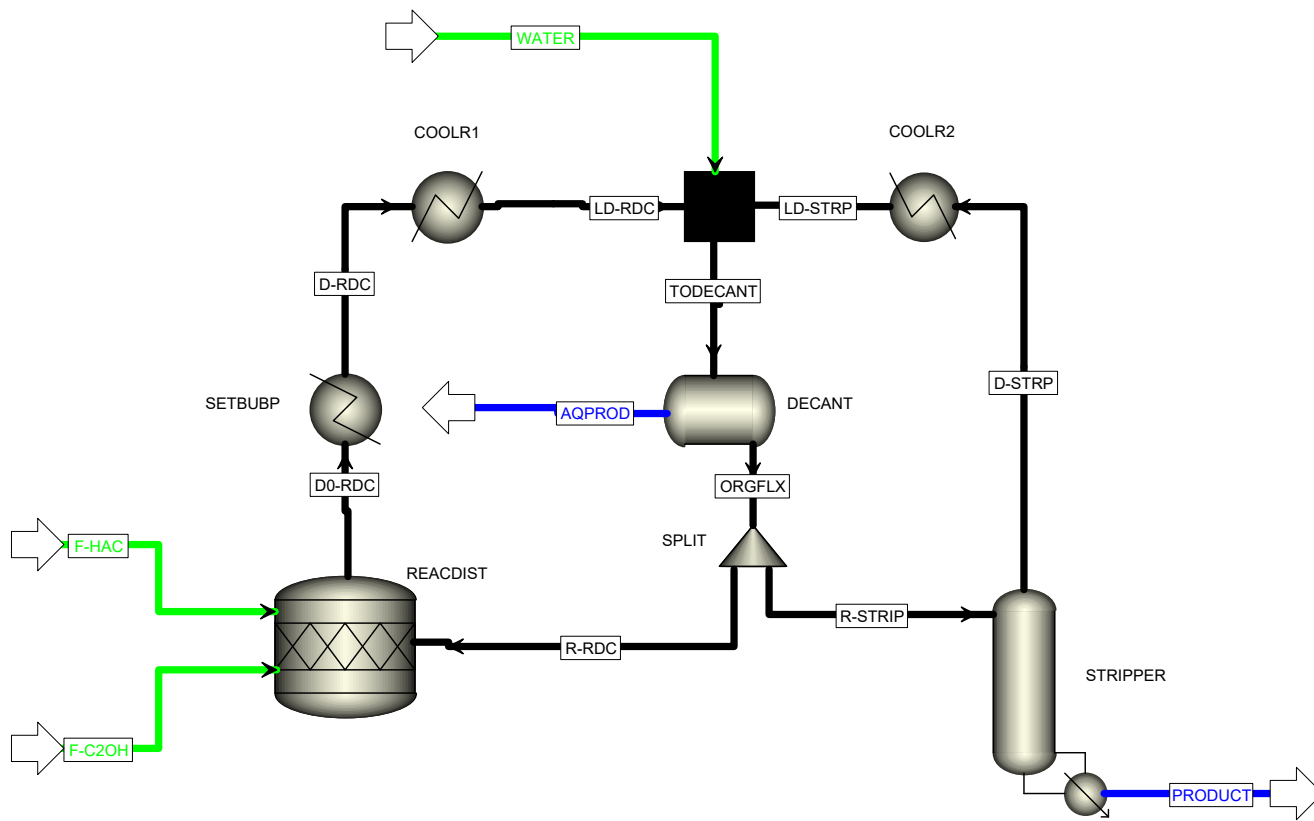


Figure 18. Aspen Plus flowsheet for ethyl acetate purification. Figure reprinted with permission from ref 45. Copyright 2017 ACS.

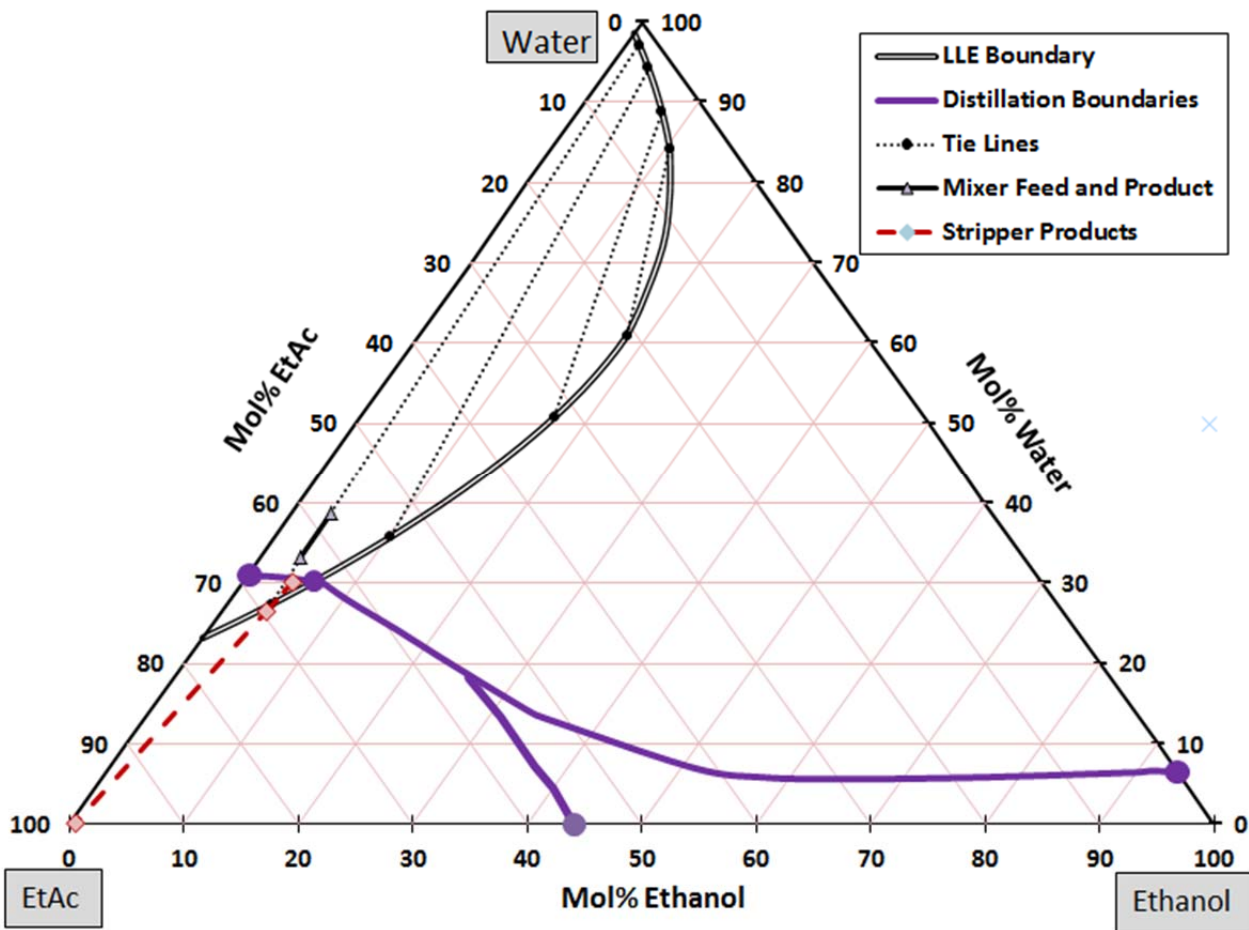


Figure 19. Ternary map of the ethyl acetate + ethanol + water system at 101.3 kPa. The double line shows the two-liquid phase boundary and the dashed lined within the dome present the tie lines. The four azeotropes are depicted by the large circles, and these identify the ends of the distillation boundaries, which divide the diagram into three regions. The small triangles show how the product from the reactive-distillation column (REACDIST) is changes after mixing with the distillate from the stripper (STRIPPER) and the water feed (WATER); this line must coincide with a tie line. The lines with the diamonds show how the feed to the stripper is separated into the product (PRODUCT) and the distillate (D-STRIP). Note that D-STRIP lies on a distillation boundary. Figure reprinted with permission from ref 45. Copyright 2017 ACS.

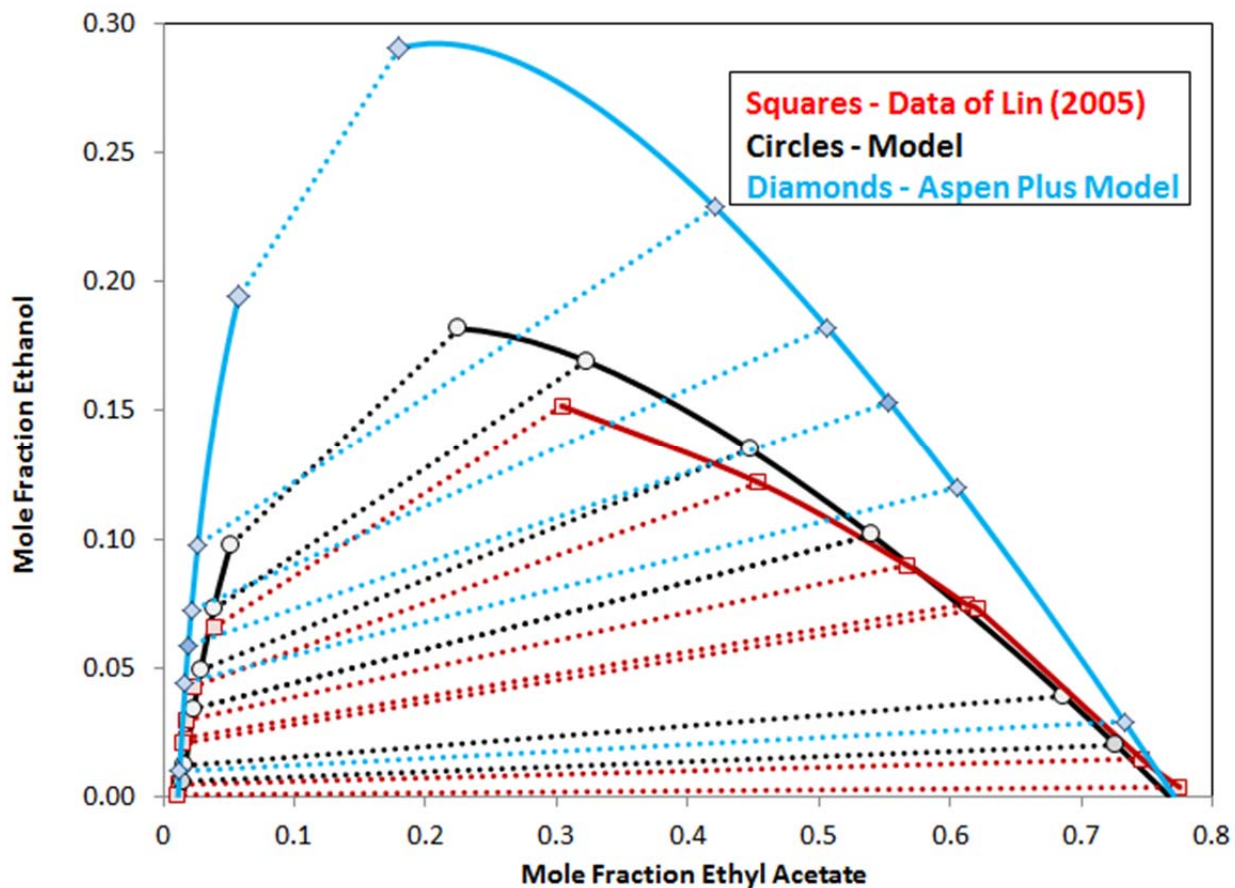


Figure 20. Liquid-liquid equilibrium in the ethyl acetate + ethanol + water ternary system at 101.3 kPa. The present model calculations (circles) and calculations from the out-of-the-box Aspen Plus model (diamonds) are compared to the data of Lee, Chen and Huang.<sup>48</sup> Figure reprinted with permission from ref 45. Copyright 2017 ACS.

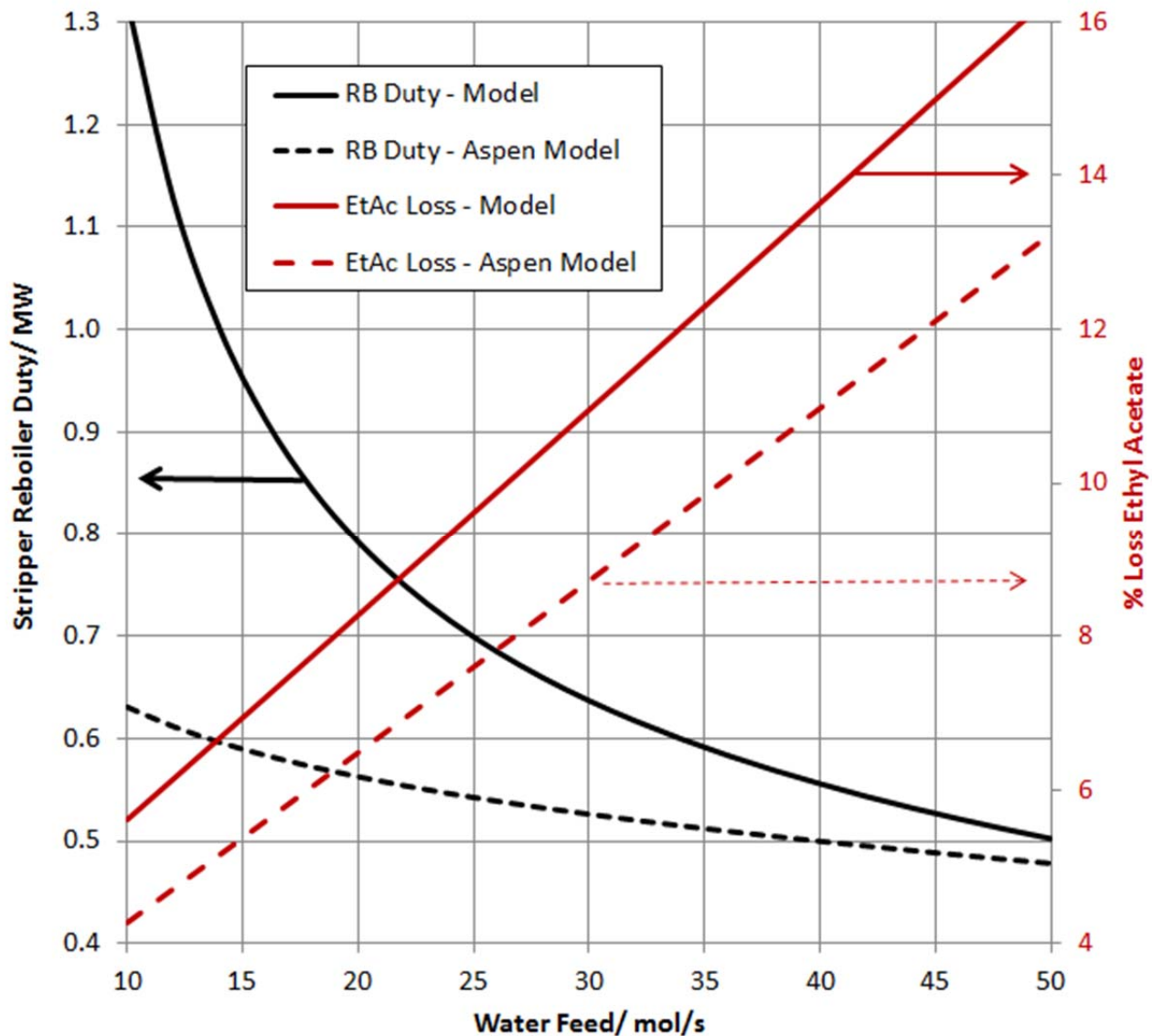


Figure 21. Effect of feed water flow on the stripper reboiler duty and the percentage ethyl acetate loss. The solid lines are results for the NRTL model developed here, while the dashed lines are for the NRTL parameters from the AspenTech database. Figure reprinted with permission from ref 45. Copyright 2017 ACS.

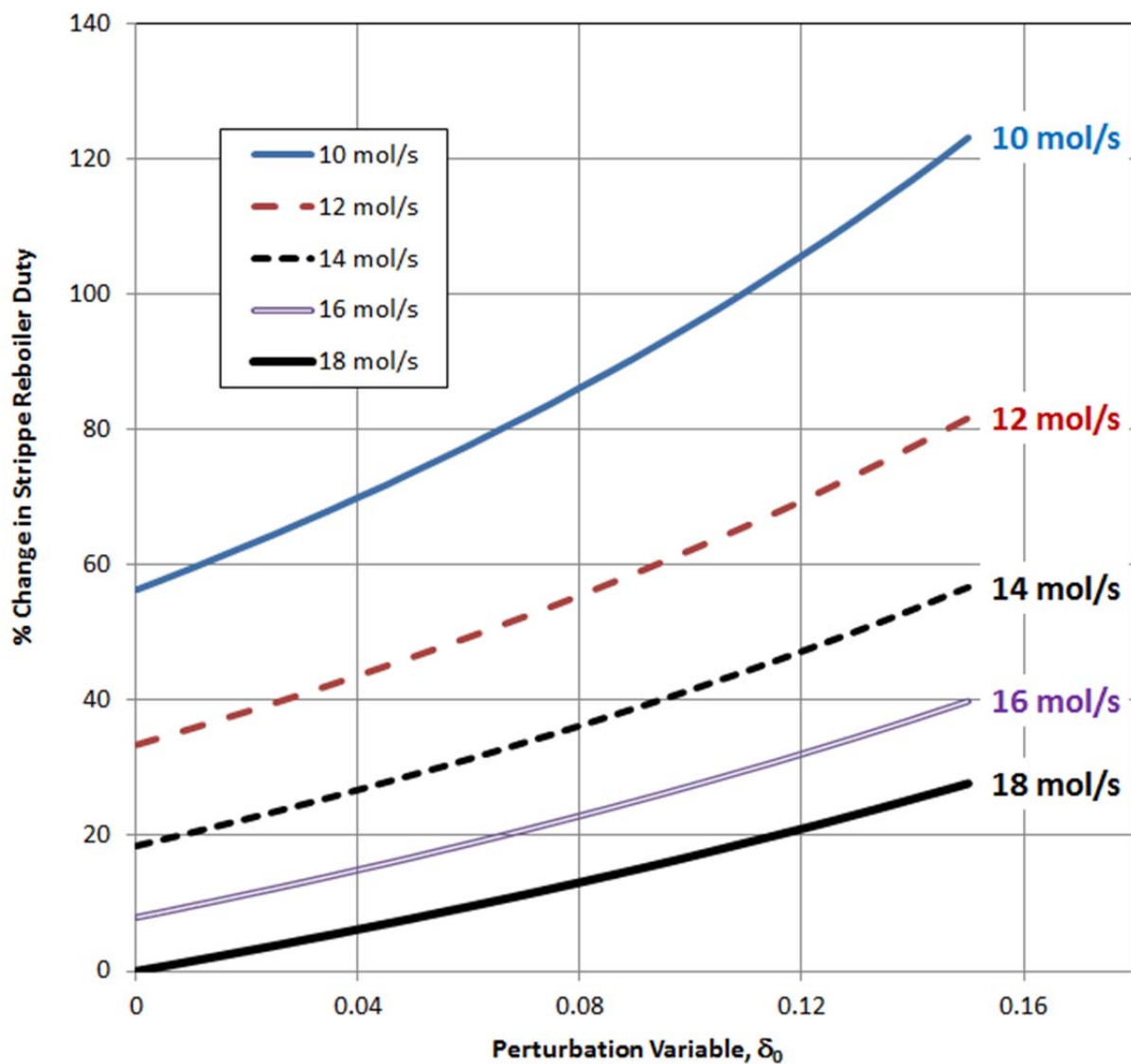


Figure 22. Effect of variation in the perturbation parameter ( $\delta_0$ ) on the stripper reboiler duty. See Figure 18 for flowsheet. Figure reprinted with permission from ref 45. Copyright 2017 ACS.

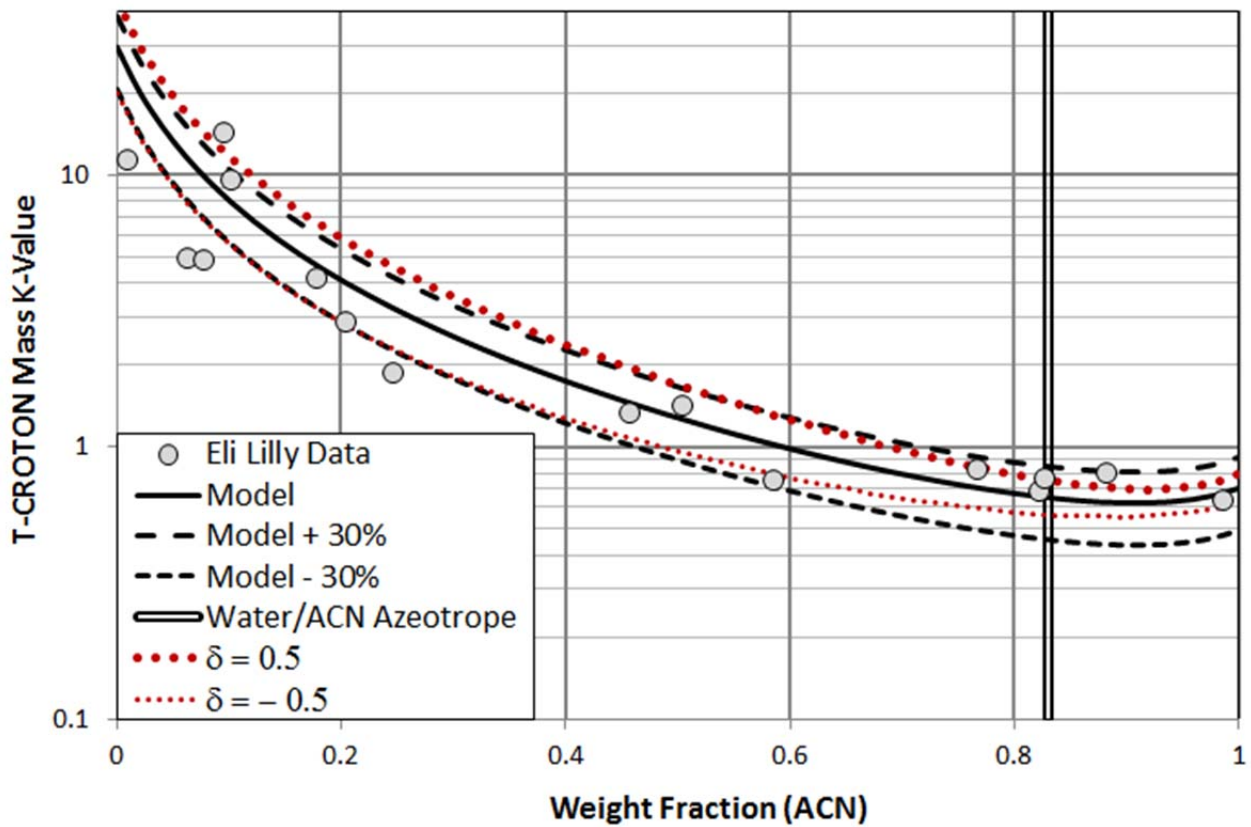


Figure 23. Mass K-Value of T-CROTON at low concentration in water + ACN at 1 atm (101.3 kPa). Comparison of model calculations to Eli Lilly data. The dashed lines show  $\pm 30\%$  from the model results. The dotted lines are model calculations with  $\delta = 0.5$  and  $\delta = -0.5$ . The vertical line indicates the water + ACN azeotrope. Figure reprinted with permission from ref 51. Copyright 2017 ACS.

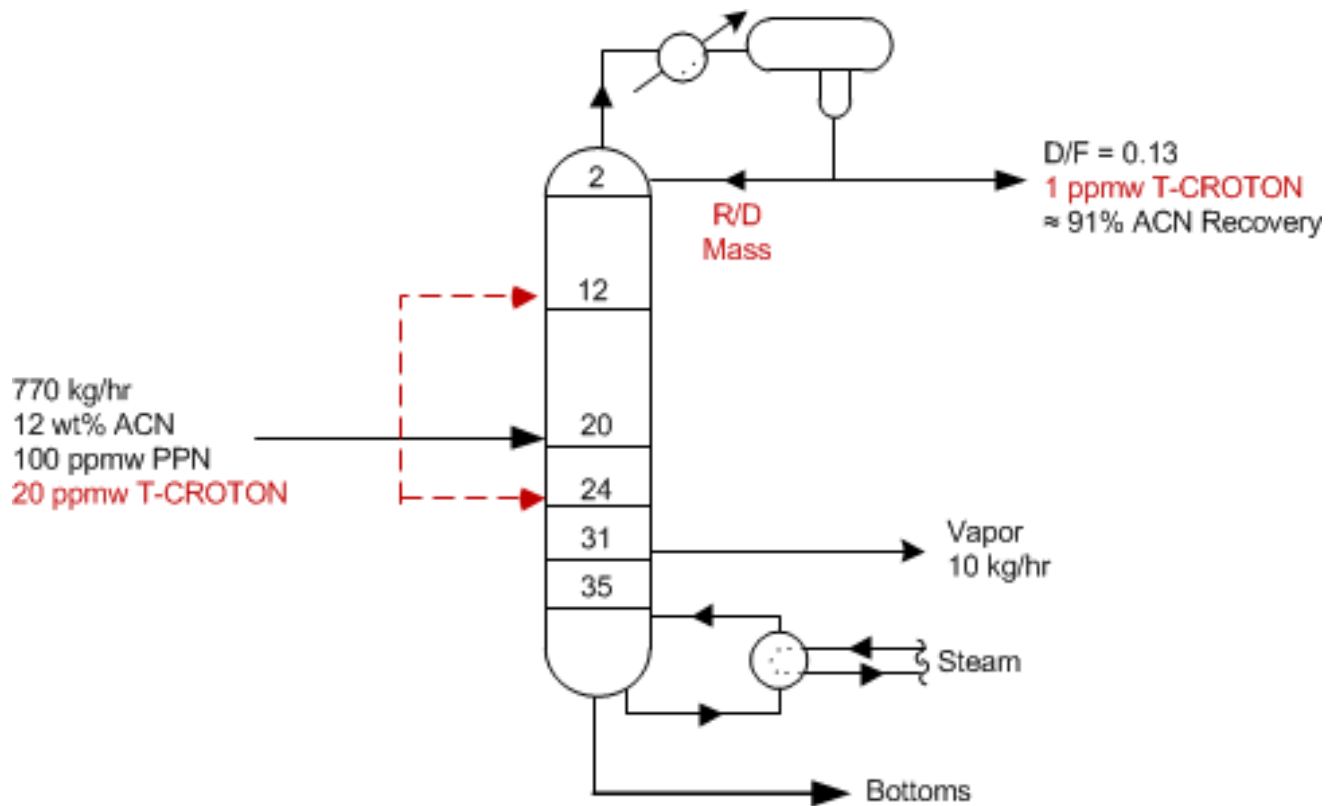


Figure 24. Single column with side draw used for component-trapping perturbation studies-1. The column operates at 1 atm (101.3 kPa). Figure reprinted with permission from ref 51. Copyright 2017 ACS.

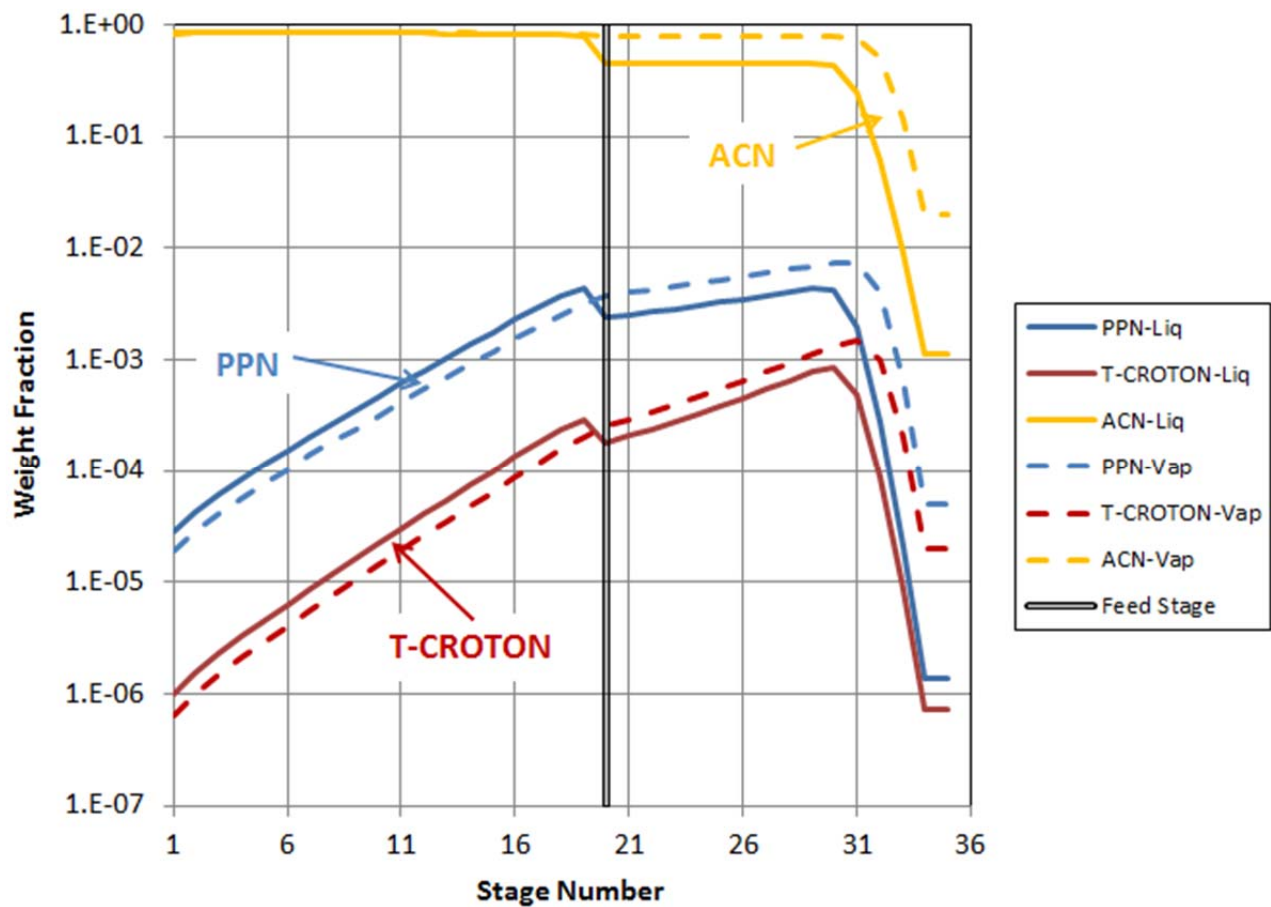
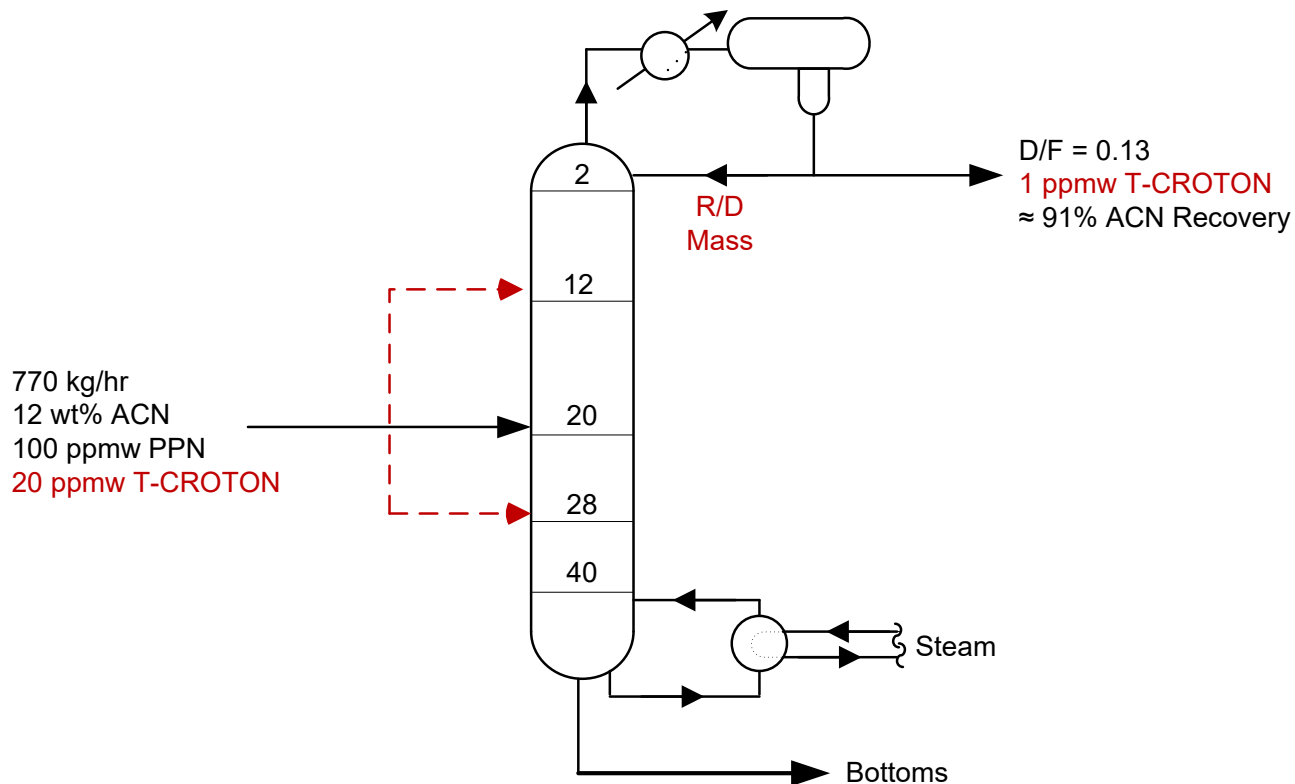


Figure 25. Vapor and liquid concentration profiles for ACN, PPN and T-CROTON in the distillation column corresponding to Figure 24, and with feed to stage 20. Figure reprinted with permission from ref 51. Copyright 2017 ACS.



**Figure 26. Single column used for component-trapping perturbation studies-2. The difference from Figure 24 is that the side draw has been eliminated. Figure reprinted with permission from ref 51. Copyright 2017 ACS.**

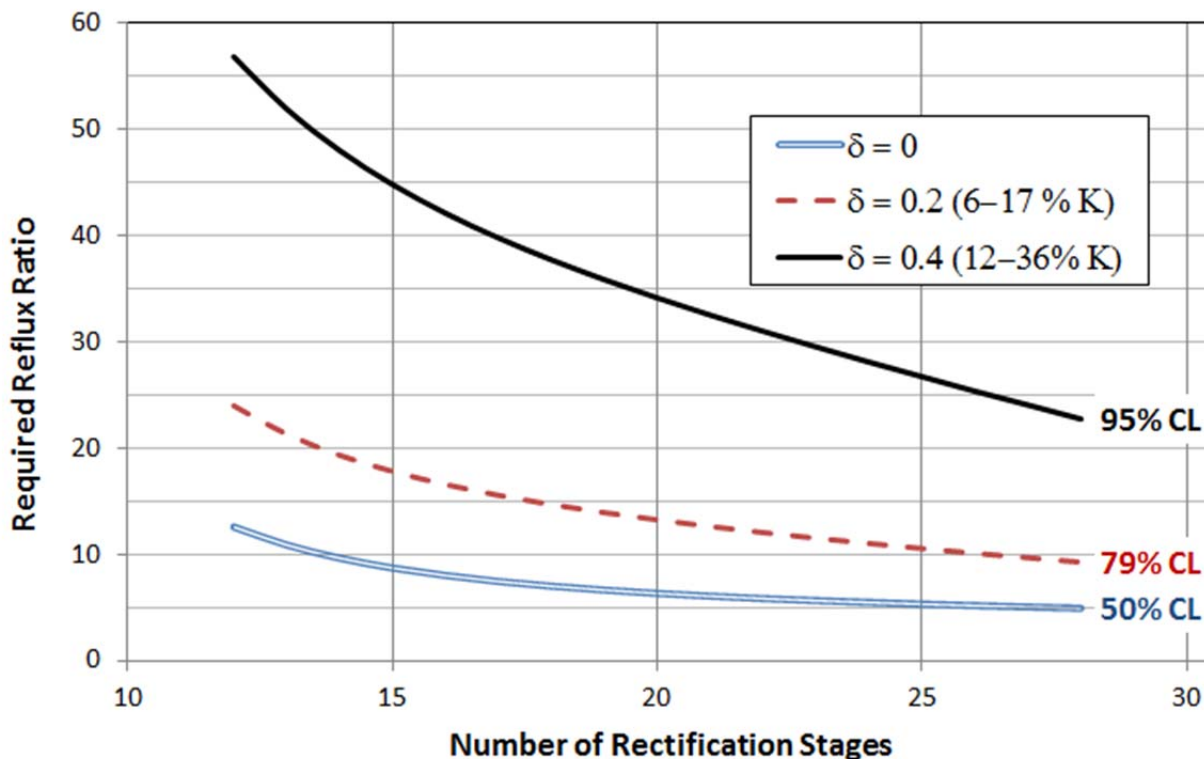


Figure 27. Effect of perturbation parameter ( $\delta$ ) and number of rectification stages on the reflux ratio required to meet the spec of 1 ppmw T-CROTON in the distillate. See Figure 26 for details. The percentage in brackets show the extent of the perturbations at the ACN-rich and water-rich ends; the water-rich end has the larger perturbation. The confidence limits (CL) are also shown for each of the three values of  $\delta$ . Figure reprinted with permission from ref 51. Copyright 2017 ACS.

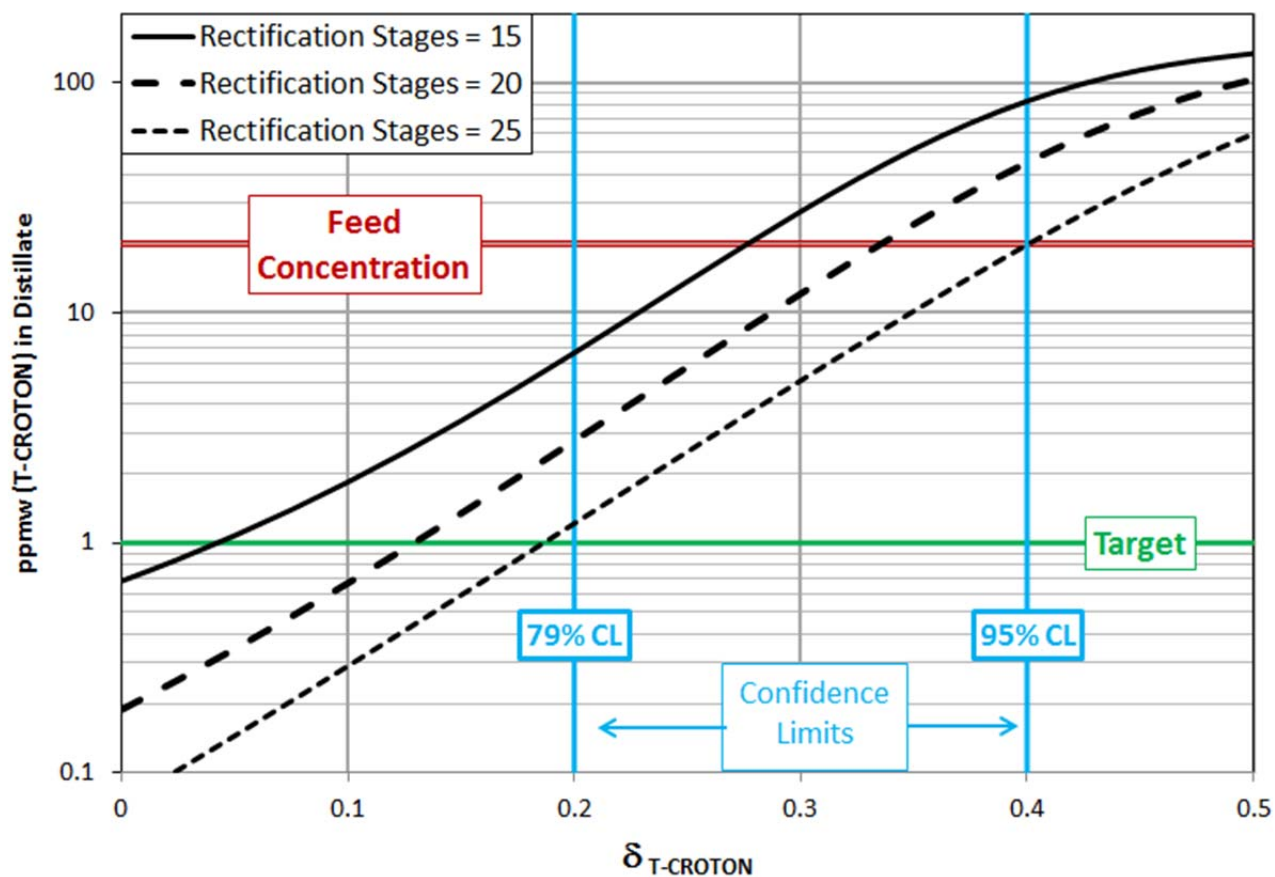


Figure 28. Effect of perturbation parameter ( $\delta$ ) and number of rectification stages on concentration of T-CROTON in distillate. Referring to Figure 26, the reflux ratio is fixed at 10. The vertical lines show the 79% and 95% confidence limits (CL); other values of CL may be estimated using Error! Reference source not found.. Figure reprinted with permission from ref 51. Copyright 2017 ACS.

## Literature Cited

---

- [1] Taylor, B. N.; Kuyatt, C. E. *Guidelines for the Evaluation and Expression of Uncertainty in NIST Measurement Results*, NIST Technical Note 1297, National Institute of Standards and Technology, Gaithersburg, MD, **1994**.
- [2] Chirico, R. D.; De Loos, T. W.; Gmehling, J.; Goodwin, A. R. H.; Gupta, S.; Haynes, W. M.; Marsh, K. N.; Rives, V.; Olson, J.; Spencer, C.; Brennecke, J. F.; Trusler, J.P.M. Guidelines for Reporting of Phase Equilibrium Measurements (IUPAC Recommendations 2012). *Pure Appl. Chem.*, **2012**, 84, 1785-1813.
- [3] Brennecke, J. F., Goodwin, A. R. H.; Mathias, P.; Wu, J. "New Procedures for Articles Reporting Thermophysical Properties," *J. Chem. Eng. Data*, **2011**, 4279.
- [4] Weir, R. D.; Trusler, J. P. M.; Pádua, A. New Procedures for Articles Reporting Thermophysical Properties, *J. Chem. Thermodyn.*, **2011**, 43,1305.
- [5] Cummings, P. T., de Loos, Th. W.; O'Connell, J. P. New Procedures for Articles Reporting Thermophysical Properties" *Fluid Phase Equil.*, **2011**, 307, iv.
- [6] Rives, V.; Schick, C.; Vyazovkin, S. New Procedures for Articles Reporting Thermophysical Properties, *Thermochim. Acta*, **2011**, 521, 1.
- [7] Haynes, W. M.; Friend, D. G.; Mandelis, A. Editorial: New Procedures for Articles Reporting Experimental Thermophysical Property Data, *Int. J. Thermophys.*, **2011**, 32, 1999-2000.
- [8] Kim, S. H.; Kang, J. W.; Kroenlein, K.; Magee, J. W.; Diky, V.; Frenkel, M. Online Resources in Chemical Engineering Education: Impact of the Uncertainty Concept from Thermophysical Properties, *Chem. Eng. Educat.*, **2013**, 47, 48-57.
- [9] Streich, M.; Kistenmacher, H. Property Inaccuracies Influence Low Temperature Designs, *Hydrocarb. Proc.*, **1979**, 58, 237-241.
- [10] Mah, R. S. H. Effects of Thermophysical Property Estimation on Process Design, *Computers Chem. Eng.*, **1977**, 1, 183-189.
- [11] Zudkevitch, D. Imprecise Data Impacts Plant Design and Operation, *Hydrocarbon Process.* **1975**, 54, 97-103.
- [12] Larsen, A. H. Data Quality for Process Design, *Fluid Phase Equilib.*, **1986**, 29, 47-58.
- [13] Zeck, S. Thermodynamics in Process Development in the Chemical Industry - Importance, Benefits, Current State and Future Development, *Fluid Phase Equilib.*, **1991**, 70, 125-140.
- [14] Macchietto, S.; Maduabeuke, G.; Szcepanski, R. Exact Determination of Process Sensitivity to Physical Properties, *Fluid Phase Equilib.*, **1986**, 29, 59-67.
- [15] Reed, M. E.; Whiting, W. B., Sensitivity and Uncertainty of Process Designs to Thermodynamic Model Parameters: A Monte Carlo Approach, *Chem. Eng. Commun.* **1993**, 124, 39-48.
- [16] Whiting, W. B.; Tong, T.-M.; Reed, M. E. Effect of Uncertainties in Thermodynamic Data and Model Parameters on Calculated Process Performance, *Ind. Eng. Chem. Res.* **1993**, 32, 1367-1371.
- [17] Whiting, W. B. Effects of Uncertainties in Thermodynamic Data and Models on Process Calculations, *J. Chem. Eng. Data*, **1996**, 41, 935-941.

- 
- [18] Whiting, W. B.; Vasquez, V. R.; Meerschaert, M. M. Techniques for Assessing the Effects of Uncertainties in Thermodynamic Models and Data, *Fluid Phase Equilib.* **1999**, 158–160, 627–641.
- [19] Xin, Y.; Whiting, W. B. Case Studies of Computer-Aided Design Sensitivity to Thermodynamic Data and Models, *Ind. Eng. Chem. Res.* **2000**, 39, 2998–3006.
- [20] Whiting, W. B.; Vasquez, V. R.; Meerschaert, M. M. Techniques for Assessing the Effects of Uncertainties in Thermodynamic Model and Data, *AIChE J.*, **1997**, 43, 440–447.
- [21] Miller, D.C. et al. Carbon Capture Simulation Initiative: A Case Study in Multiscale Modeling and New Challenges. *Annu. Rev. Chem. Biomol. Eng.*, **2014**, 5, 301-323.
- [22] Fair, J. R., Advanced Process Engineering, *AIChE Monograph Series*, **1980**, 76, 13-
- [23] Poling, B. E.; Prausnitz, J. M.; O’Connell, J. P. *The Properties of Gases and Liquids*; McGraw Hill Professional, New York, 2000.
- [24] Mathias, P. M., Sensitivity of Process Design to Phase Equilibrium – A New Perturbation Method Based Upon the Margules Equation. *J. Chem. Eng. Data*, **2014**, 59, 1006-1015.
- [25] Renon, H.; Prausnitz, J. M. Local Compositions in Thermodynamic Excess Functions for Liquid Mixtures. *AIChE J.*, **1968**, 14, 135-144.
- [26] Redlich, O.; Kwong, J. N. S. On the Thermodynamics of Solutions. V An Equation of State. Fugacities of Gaseous Solutions. *Chem. Rev.*, **1949**, 44, 233-244.
- [27] Rowley, R. L.; Wilding, W. V.; Oscarson, J. L.; Yang, Y.; Zundel, N. A. DIPPR® *Data Compilation of Pure Chemical Properties*, Design Institute for Physical Properties, AIChE, New York, NY, **2010**.
- [28] Frenkel, M.; Chirico, R. D.; Diky, V.; Yan, X.; Dong, Q.; Muzny, C. ThermoData Engine (TDE): Software Implementation of the Dynamic Data Evaluation Concept. *J. Chem. Inf. Model.*, **2005**, 45, 816-838. TDE is also available online at <http://trc.nist.gov/tde.html>.
- [29] Onken U.; Rarey J.; Gmehling J. The Dortmund Data Bank: A Computerized System for Retrieval, Correlation, and Prediction of Thermodynamic Properties of Mixtures. *Int. J. Thermophys.*, **1989**, 10, 739-747. DDB is also available online at <http://www.ddbst.com/ddb.html>.
- [30] UNIFAC is an estimation method based upon group contributions. Several UNIFAC models are available in Aspen Plus V8.8. In the present study, since mainly approximate estimations are required, the base UNIFAC model has been used. Fredenslund, Aa.; Gmehling, J.; and Rasmussen, P. *Vapor-Liquid Equilibria Using UNIFAC, A Group-Contribution Method*, 3<sup>rd</sup> Impression, Elsevier, Amsterdam, **1977**.
- [31] Mathias, P. M. Guidelines for the Analysis of Vapor-Liquid Equilibrium Data. *J. Chem. Eng. Data*, **2017**, 62, 2231-2233.
- [32] Kojima, K.; Tochigi, K.; Kurihara, K.; Nakamichi, M. Isobaric Vapor- Liquid Equilibria for Acetone + Chloroform + Benzene and the Three Constituent Binary Systems. *J. Chem. Eng. Data* **1991**, 36, 343-345.
- [33] Kudryavtseva, L. S.; Susarev, M. P. Liquid-Vapor Equilibrium in Chloroform-Hexane and Acetone-Chloroform Systems. *Zh. Prikl. Khim. (Leningrad)* **1963**, 36, 1231-1237.
- [34] Kogan, L. V.; Deizenrot, I. V. Apparatus for Determination of Liquid-Vapor Equilibrium in Systems with Nonideal Vapor Phases. *Zh. Prikl. Khim. (Leningrad)* **1975**, 48, 2757-2759.

- 
- [35] Segura, H.; Mejia, A.; Reich, R.; Wisniak, J.; Loras, S. Isobaric Vapor-Liquid Equilibria and Densities for the Binary Systems Oxolane + Ethyl 1,1-Dimethylethyl Ether, Oxolane + 2-Propanol and Propan-2-One + Trichloromethane. *Phys. Chem. Liq.* **2003**, 41, 283-301.
- [36] Reinders, W.; de Minjer, C. H. Vapour-Liquid Equilibria in Ternary Systems. II. The System Acetone-Chloroform-Benzene. *Rec. Trav. Chim.* **1940**, 49, 369-391.
- [37] Mathias, P. M. Effect of VLE Uncertainties on the Design of Separation Sequences by Distillation – Study of the Benzene-Chloroform-Acetone System. *Fluid Phase Equilib.*, **2016**, 408, 265-272.
- [38] Westerberg, A. W.; Wahnschafft, O. Synthesis of Distillation-Based Separation Systems. *Adv. Chem. Eng.*, **1996**, 23, 63-170.
- [39] Hoffman, E. J. *Azeotropic and Extractive Distillation*; Wiley (Interscience), New York, **1964**.
- [40] Doherty, M. F.; Perkins, J. D. On the Dynamics of Distillation Processes—I: The Simple Distillation of Multicomponent Non-reacting, Homogeneous Liquid Mixtures. *Chem. Eng. Sci.*, **1978**, 33, 281-301.
- [41] For further descriptions on how to use the multiple dataset capability refer to the Aspen Plus documentation available from Aspen Technology, Inc.
- [42] Mathias, P. M. Effect of Phase-Equilibrium Uncertainties on the Separation of Heterogeneous Azeotropes – Application to the Water/1-Butanol System. *J. Chem. Eng. Data*, **2016**, 61, 4077-4084.
- [43] Maczynski, A.; Shaw, D. C., Goral, M.; Wisniewska-Gocłowska, B. IUPAC-NIST Solubility Data Series. 82. Alcohols with Water—Revised and Updated: Part 1. C4 Alcohols with Water. *J. Phys. Chem. Ref. Data*, **2007**, 36, 59-132.
- [44] van der Merwe, A. B.; Cheng, H.; Görgens, J. F.; Knoetze, J. H. Comparison of Energy Efficiency and Economics of Process Designs for Biobutanol Production from Sugarcane Molasses. *Fuel*, **2013**, 105, 451–458.
- [45] Mathias, P. M.; Kister, H. Z. Effect of Phase-Equilibrium Uncertainties on Ethyl Acetate Purification, *J. Chem. Eng. Data*, **2017**, 62, 2872-2883.
- [46] Keyes, D. B. Esterification processes and Equipment. *Ind. Eng. Chem.*, **1932**, 24, 1096–1103.
- [47] Tang, Y. T.; Huang, H.-P.; Chien, I.-L. Design of a Complete Ethyl Acetate Reactive Distillation Column System. *Computer Aided Chem. Eng.*, **2003**, 15, 1044–1049.
- [48] Lee, L.-S.; Chen, W.-C.; Huang, J.-F. Experiments and Correlations of Phase Equilibria of Ethanol-Ethyl Acetate-Water Ternary Mixture. *J. Chem. Eng. Jpn.*, **1996**, 29, 427-438.
- [49] Kister, H. Z. Components Trapping in Distillation Towers: Causes, Symptoms and Cures,” *Chem. Eng. Prog.* **2004**, 100, 22-33
- [50] Kister, H. Z. *Distillation Troubleshooting*. John Wiley and Sons, Inc., Hoboken, NJ, **2006**
- [51] Mathias, P. M.; Kister, H, Z.; Parker, B.; Narvaez, L.; Schafer, T.; Erickson, A. Component Trapping with VLE Uncertainty: Principles, Design and Troubleshooting. *Ind. Eng. Chem. Res.* **2017**, 56, 11593-11602.
- [52] Parker, B. Data measured in Eli Lilly Corporate Center Laboratory, August, **2016**
- [53] Chirico, R. D.; Frenkel M.; Diky, V.; Marsh, K. N.; Wilhoit R. C. ThermoML - An XML-Based Approach for Storage and Exchange of Experimental and Critically Evaluated Thermophysical and Thermochemical Property Data. 2. Uncertainties. *J. Chem. Eng. Data*, **2003**, 48, 1344-1359.

---

[54] Abramowitz, M.; Stegun, I. A. *Handbook of Mathematical Functions: with Formulas, Graphs, and Mathematical Tables*; Dover Publications, Inc., New York, **1964**.

[55] Note that a total condenser does not function as a distillation stage since no fractionation occurs (see Figure 24 and Figure 26). However, it is counted as a stage in Aspen Plus, and this convention has been retained.